

LDLT \mathcal{L} -Lipschitz Network: Generalized Deep End-To-End Lipschitz Network Construction

Marius F. R. Juston

MJUSTON2@ILLINOIS.EDU

*The Grainger College of Engineering, Industrial and Enterprise Systems Engineering Department
University of Illinois Urbana-Champaign
Urbana, IL 61801-3080, USA*

Ramavarapu S. Sreenivas

RSREE@ILLINOIS.EDU

*The Grainger College of Engineering, Industrial and Enterprise Systems Engineering Department
University of Illinois Urbana-Champaign
Urbana, IL 61801-3080, USA*

Dustin Nottage

DUSTIN.S.NOTTAGE@ERDC.DREN.MIL

*Construction Engineering Research Laboratory
U.S. Army Corps of Engineers Engineering Research and Development Center
Urbana, IL 61822, USA*

Ahmet Soylemezoglu

AHMET.SOYLEMEZOGLU@ERDC.DREN.MIL

*Construction Engineering Research Laboratory
U.S. Army Corps of Engineers Engineering Research and Development Center
Urbana, IL 61822, USA*

Editor: My editor

Abstract

Deep residual networks (ResNets) have demonstrated outstanding success in computer vision tasks, attributed to their ability to maintain gradient flow through deep architectures. Simultaneously, controlling the Lipschitz constant in neural networks has emerged as an essential area of research to enhance adversarial robustness and network certifiability. This paper presents a rigorous approach to the general design of \mathcal{L} -Lipschitz deep residual networks using a Linear Matrix Inequality (LMI) framework. Initially, the ResNet architecture was reformulated as a cyclic tridiagonal LMI, and closed-form constraints on network parameters were derived to ensure \mathcal{L} -Lipschitz continuity; however, using a new LDL^T decomposition approach for certifying LMI feasibility, we extend the construction of \mathcal{L} -Lipschitz networks to any other nonlinear architecture. Our contributions include a provable parameterization methodology for constructing Lipschitz-constrained residual networks and other hierarchical architectures. Cholesky decomposition is also used for efficient parameterization. These findings enable robust network designs applicable to adversarial robustness, certified training, and control systems. The LDL^T formulation is shown to be a tight relaxation of the SDP-based network, maintaining full expressiveness and achieving 3%-13% accuracy gains over SLL Layers on 121 UCI data sets.

Keywords: Lipschitz neural networks, linear matrix inequalities, residual networks, certified robustness, nonlinear systems

1 Introduction

The robustness of deep neural networks (DNNs) is a critical challenge, particularly in safety-sensitive domains where small adversarial perturbations can lead to dangerous outcomes, such as the misclassification of important objects. One approach to address this issue is by enforcing Lipschitz constraints on the network architectures. These constraints ensure that small changes in the input do not significantly alter the output. This property is vital for certifying robustness against adversarial attacks, which involve introducing slight noise to modify the expected classification output result (Inkawhich et al., 2019; Goodfellow et al., 2014). The Lipschitz constant is a key measure to bound the network’s sensitivity to input perturbations. Specifically, a \mathcal{L} -Lipschitz network can be theoretically guaranteed to remain stable within a defined “stability sphere” around each input, making it resistant to adversarial attacks up to a certain magnitude (Tsuzuku et al., 2018).

To achieve this, several methods have been proposed to enforce Lipschitz constraints on neural networks, including spectral normalization (Miyato et al., 2018; Bartlett et al., 2017), orthogonal parameterization (Prach and Lampert, 2022), and more recent approaches such as Convex Potential Layers (CPL) and Almost-Orthogonal Layers (AOL) (Meunier et al., 2022; Prach and Lampert, 2022). Previous works have been formulated under a unifying semidefinite programming architecture that imposes constraints on the networks as LMIs (Araujo et al., 2023). From the SDP programming architecture, the SDP-based Lipschitz layers (SLL) from Araujo et al. (2023) and most recently the Sandwich layers (Wang and Manchester, 2023), monotone Deep Equilibrium Models (DEQ) (MonDEQ) (Winston and Zico Kolter, 2020), and Lipschitz-bounded equilibrium models (LBEN) (Havens et al., 2023) have emerged. Havens et al. (2023) further shows how various Lipschitz structures (CPL, SLL, AOL, and Sandwich) interact in the DEQ setting. Our LDL^\top construction could yield additional structures that DEQs can exploit, generalizing the methodology. However, ensuring Lipschitz constraints in deep architectures, particularly residual networks (ResNets), presents unique challenges due to their recursive structure. While prior work has made strides in constraining individual layers (Araujo et al., 2023; Meunier et al., 2021a) and in developing a unifying semidefinite programming approach, the generalized deep residual network formulation presents issues due to the pseudo-tri-diagonal structure of the LMI it imposes. Our formulation can be viewed as an extension of the unified SDP-based perspective of Araujo et al. (2023) to deep residual modules and multi-layered sub-systems, using block LDL^\top factorization of the resulting LMI.

Furthermore, multi-layered general Feedforward Neural Networks (FNN) have been shown to generate block tri-diagonal matrix LMI formulations (Xu and Sivaranjani, 2024; Wang and Manchester, 2023) due to their inherent network structure, which, in contrast to the residual formulation, yield explicit solutions (Sandryhaila and Moura, 2013; Agarwal et al., 2019). However, due to the residual network’s off-diagonal structure, applying the exact eigenvalue computation directly is not feasible, making the solution process significantly more complex.

Previous work has also demonstrated an iterative approach by using projected gradient descent or a regularization term on the estimated Lipschitz constant to enforce a constraint on the Lipschitz constant (Gouk et al., 2021; Aziznejad et al., 2020; Bear et al., 2024). While this guarantees an iterative enforcement of the Lipschitz constraint, it does not ensure a

theoretical Lipschitz guarantee across the entire network until this convergence. However, the advantage of this technique is its generalizability, which allows for the usage of more general network structures.

1.1 Contributions

This paper introduces the formulation of deep residual networks as Linear Matrix Inequalities (LMI). It derives closed-form constraints on network parameters to ensure theoretical \mathcal{L} -Lipschitz constraints. The LMI was structured as a tri-diagonal matrix with off-diagonal components, which inherently complicates the derivation of closed-form eigenvalue computations.

Moreover, while Araujo et al. (2023)’s work generates a closed-form solution for a residual network, it is limited to considering a single inner layer. In contrast, this paper presents a more general formulation that accommodates a more expressive inner-layer system within the residual network, offering greater flexibility and broader applicability.

This method decomposes the LMI system into an LDL^\top formulation and restricts the diagonal matrix D to be strictly positive definite. Formally, we show in Sections 3.1 to 3.3 that for fixed architecture and Lipschitz constant \mathcal{L} , the feasible set of LDL^\top -parameterized weights coincides with the feasible set of the SDP problem from Fazlyab et al. (2019b), restricted to general hierarchical neural network architectures. It is illustrated specifically in this paper for the cyclic block-tri-diagonal LMI (up to measure-zero degeneracies). This implies that our parameterization is a tight reparameterization of the SDP-based bound in the sense of Wang and Manchester (2023); Araujo et al. (2023), rather than formulating the network as a composition of 1-Lipschitz layers. This allows the system to be viewed as an end-to-end parameterization and generalizes the architectures of the 1-Lipchitz formulation from Fazlyab et al. (2019b); Araujo et al. (2023); Wang and Manchester (2023). Providing a standard decomposition methodology for any compositional or hierarchical non-linear system.

Efficient computation optimizations were derived for the LDL^\top parameterization by converting the square root of the matrix operation, which is extremely expensive for large-dimensional matrices, into Cholesky decomposed triangular matrices.

Empirical comparisons with the current state of the art are provided on tabular classification benchmarks, 121 curated UCI data sets, with certified accuracies at different levels across algorithms statistically compared.

2 LMI Formulation

Following the work of Araujo et al. (2023), who formulated a Lipschitz neural network as a constrained LMI problem to construct a residual network, limitations in their approach were identified. Specifically, their formulation yielded a single-layer residual network, which is inherently less expressive than the generalized deep-layered residual network popularized by architectures such as ResNet and its variants (He et al., 2015b; Szegedy et al., 2016; Zagoruyko and Komodakis, 2016; Hu et al., 2017; Xie et al., 2016). These deeper networks perform better because the multiple inner layers within the modules enable more complex latent-space transformations, thereby increasing the network’s expressiveness. This research focuses on establishing constraints for the inner layers to maintain the \mathcal{L} -Lipschitz condition

while maximizing the expressiveness of the residual network for larger inner layers. As such, the inner layers of the residual network were represented as a recursive system of linear equations:

$$\begin{aligned} x_{k+1} &= A_k x_k + B_k w_{k,n}, \\ v_{k,n} &= C_n w_{k,n-1} + b_n, \\ w_{k,n} &= \sigma_n(v_{k,n}), \\ &\vdots \\ v_{k,1} &= C_1 x_k + b_1, \\ w_{k,1} &= \sigma_1(v_{k,1}). \end{aligned}$$

Where each of the layer parameters were defined as $C_l \in \mathbb{R}^{d_l \times d_{l-1}}$, $b_l \in \mathbb{R}^{d_l}$ for $l \in \{1, \dots, n\}$. When $n = 1$, the formulation reduces to the one presented in Araujo et al. (2023), rendering it redundant in its derivation. The goal of the LMI was to maintain the Lipschitz constraint formulated as $\|x'_{k+1} - x_{k+1}\| \leq \mathcal{L}\|x'_k - x_k\|$.

Given that this system could be represented as a large recursive system, it was possible to split all the constraints of the inner layers as a set of LMI conditions similar to Araujo et al. (2023); Xu and Sivaranjani (2024); Fazlyab et al. (2019a).

We only require that each non-linear function, in this case the activation functions, satisfy a pointwise slope restriction, which can be encoded via incremental quadratic constraints (IQC) as in Xu and Sivaranjani (2024); Araujo et al. (2023); Lessard et al. (2015); Fazlyab et al. (2019b); Megretski and Rantzer (1997). Strong convexity is not required; in particular, ReLU and leaky ReLU fit in this framework with $m_i = 0$ and $L_i = 1$. The full parameterization of available activation functions can be found in Appendix A. The IQC is defined as:

$$\begin{bmatrix} v_k - v'_k \\ w'_{k,i} - w_{k,i} \end{bmatrix}^\top \begin{bmatrix} -2L_i m_i \Lambda_i & (m_i + L_i) \Lambda_i \\ (m_i + L_i) \Lambda_i & -2\Lambda_i \end{bmatrix} \begin{bmatrix} v_k - v'_k \\ w'_{k,i} - w_{k,i} \end{bmatrix} \leq 0,$$

where Λ_n must be a positive definite diagonal matrix. Given that $v_k - v'_k = C_n(w_{k,n-1} - w'_{k,n-1})$ the inequality thus becomes the following quadratic constraints, where $\Delta w_{k,i}$ was defined as $\Delta w_{k,i} = w'_{k,i} - w_{k,i}, \forall i \in \{1, 2, \dots, n\}$,

$$\begin{bmatrix} C_i(\Delta w_{k,i-1}) \\ \Delta w_{k,i} \end{bmatrix}^\top \begin{bmatrix} -2L_i m_i \Lambda_i & (m_i + L_i) \Lambda_i \\ (m_i + L_i) \Lambda_i & -2\Lambda_i \end{bmatrix} \begin{bmatrix} C_i(\Delta w_{k,i-1}) \\ \Delta w_{k,i} \end{bmatrix} \leq 0.$$

The following LMI could be formulated as the summation in Equation (1).

$$\begin{bmatrix} x'_k - x_k \\ w'_{k,1} - w_{k,1} \\ w'_{k,2} - w_{k,2} \\ \vdots \\ w'_{k,n-1} - w_{k,n-1} \\ w'_{k,n} - w_{k,n} \end{bmatrix}^\top \begin{bmatrix} \mathbf{I}_{d_x} & \mathbf{0}_{d_x} \\ \vdots & \mathbf{0}_{d_1} \\ \vdots & \vdots \\ \vdots & \vdots \\ \mathbf{0}_{d_{n-1}} & \vdots \\ \mathbf{0}_{d_x} & \mathbf{I}_{d_x} \end{bmatrix} \begin{bmatrix} A_k^\top A_k - \mathcal{L}^2 \mathbf{I} & A_k^\top B_k \\ B_k^\top A_k & B_k^\top B_k \end{bmatrix} \begin{bmatrix} \mathbf{I}_{d_x} & \mathbf{0}_{d_x} \\ \vdots & \mathbf{0}_{d_1} \\ \vdots & \vdots \\ \vdots & \vdots \\ \mathbf{0}_{d_{n-1}} & \vdots \\ \mathbf{0}_{d_x} & \mathbf{I}_{d_x} \end{bmatrix}^\top \begin{bmatrix} x'_k - x_k \\ w'_{k,1} - w_{k,1} \\ w'_{k,2} - w_{k,2} \\ \vdots \\ w'_{k,n-1} - w_{k,n-1} \\ w'_{k,n} - w_{k,n} \end{bmatrix} +$$

$$\sum_{l=1}^n \begin{bmatrix} x'_k - x_k \\ w'_{k,1} - w_{k,1} \\ w'_{k,2} - w_{k,2} \\ \vdots \\ w'_{k,n-1} - w_{k,n-1} \\ w'_{k,n} - w_{k,n} \end{bmatrix}^\top E_i^\top \begin{bmatrix} C_l & \mathbf{0} \\ \mathbf{0} & \mathbf{I} \end{bmatrix}^\top \begin{bmatrix} -2L_l m_l \Lambda_l & (m_l + L_l) \Lambda_l \\ (m_l + L_l) \Lambda_l & -2\Lambda_l \end{bmatrix} \begin{bmatrix} C_l & \mathbf{0} \\ \mathbf{0} & \mathbf{I} \end{bmatrix} E_i \begin{bmatrix} x'_k - x_k \\ w'_{k,1} - w_{k,1} \\ w'_{k,2} - w_{k,2} \\ \vdots \\ w'_{k,n-1} - w_{k,n-1} \\ w'_{k,n} - w_{k,n} \end{bmatrix} \leq 0, \quad (1)$$

where,

$$D_l = \sum_{i=1}^l d_i, \quad E_l : \{0, 1\}^{(d_l + d_{l-1}) \times D_n}, \text{ and } [E_l]_{ij} = \begin{cases} 1, & \text{if } j - D_l = i \\ 0, & \text{else} \end{cases},$$

moreover, i and j represented the row and column indices, respectively. The E_l matrix represented a “selection” vector to ensure that the proper variables were used for the parameterization, which gave the following LMI in Equation (2).

$$\begin{bmatrix} A^\top A - \mathcal{L}^2 \mathbf{I} - 2L_1 m_1 C_1^\top \Lambda_1 C_1 & (L_1 + m_1) C_1^\top \Lambda_1 & \mathbf{0} & \mathbf{0} & \mathbf{0} & A^\top B \\ (L_1 + m_1) \Lambda_1 C_1 & -2L_2 m_2 C_2^\top \Lambda_2 C_2 - 2\Lambda_1 & \ddots & \mathbf{0} & \mathbf{0} & \mathbf{0} \\ \mathbf{0} & \ddots & \ddots & \ddots & \mathbf{0} & \mathbf{0} \\ \mathbf{0} & \mathbf{0} & \ddots & \ddots & \ddots & \mathbf{0} \\ \mathbf{0} & \mathbf{0} & \mathbf{0} & \ddots & -2L_n m_n C_n^\top \Lambda_n C_n - 2\Lambda_{n-1} & (L_n + m_n) C_n^\top \Lambda_n \\ B^\top A & \mathbf{0} & \mathbf{0} & \mathbf{0} & (L_n + m_n) \Lambda_n C_n & B^\top B - 2\Lambda_n \end{bmatrix} \preceq \mathbf{0} \quad (2)$$

We seek a parameterization of $A, \{\Lambda_1, \dots, \Lambda_n\}, \{C_1, \dots, C_n\}$, and B that ensures the LMI was indeed negative semidefinite to satisfy the Lipschitz constraint where ideally $\{C_1, \dots, C_n\}$ would be as unconstrained as possible to ensure expressive inner layers. From the LMI, it was discovered that explicitly deriving the network’s constraint based on its eigenvalues proved to be an exceptionally intricate task.

3 LDL Decomposition

The sparse block structure of the LMI allows the exploration of potential decompositions that would lend to a more straightforward solution. Given that we know that Equation (2) should be constructed as a positive semidefinite symmetric matrix, we can thus find a decomposition that would allow for a nice block structure, which would make it feasible to bound the eigenvalue signs quickly. Such a candidate is the Cholesky LDL^\top decomposition, also known as the real square-root-free Cholesky decomposition.

Theorem 1 *Given a real symmetric positive-definite matrix, the factorization may be written as*

$$\mathbf{A} = \mathbf{L} \mathbf{D} \mathbf{L}^\top,$$

where \mathbf{L} is a lower unit triangular (unitrangular) matrix, and \mathbf{D} is a (block) diagonal matrix. If \mathbf{A} is positive definite, then \mathbf{D} will also be positive definite (Watkins, 2002). Where the

following recursive relations apply for the entries of \mathbf{D} and \mathbf{L} :

$$\mathbf{D}_j = \mathbf{A}_{jj} - \sum_{k=1}^{j-1} \mathbf{L}_{jk} \mathbf{D}_k \mathbf{L}_{jk}^\top, \quad (\text{LD1})$$

$$\mathbf{L}_{ij} = \left(\mathbf{A}_{ij} - \sum_{k=1}^{j-1} \mathbf{L}_{ik} \mathbf{D}_k \mathbf{L}_{jk}^\top \right) \mathbf{D}^{-1}, \quad \text{for } i > j. \quad (\text{LD2})$$

An advantage of the LDL^\top decomposition over the traditional Cholesky decomposition, which Wang and Manchester (2023) alluded to, is the absence of the need to compute the square root of components. This simplification facilitates the computation and derivation of the necessary components for this system and enables a more straightforward formulation for the block variant form. Given this block factorization, we can examine the current LMI in Equation (2), and decompose each of its elements. However, since the current LMI assumes negative semidefiniteness, we must ensure that we reverse the sign of the matrix as $M \preceq \mathbf{0} \Leftrightarrow -M \succeq \mathbf{0}$.

For our application, given that we only need the system's positive definiteness to be enforced, it is only necessary to constrain all the \mathbf{D}_i such that $\mathbf{D}_i \succeq \mathbf{0}$ for all $i \in \mathbb{N}$.

3.1 Block Decompositions

The LMI is defined as a block matrix of $(n+1) \times (n+1)$ blocks,

Lemma 2 *The result of \mathbf{D}_1 is equal to the symmetric matrix,*

$$\mathbf{D}_1 = \mathcal{L}^2 \mathbf{I} + 2\mathbf{L}_1 m_1 \mathbf{C}_1^\top \Lambda_1 \mathbf{C}_1 - \mathbf{A}^\top \mathbf{A},$$

additionally,

Lemma 3 *The result of \mathbf{D}_j for $j \in \{2, \dots, n\}$ is equal to the symmetric matrix,*

$$\mathbf{D}_j = 2\mathbf{L}_j m_j \mathbf{C}_j^\top \Lambda_j \mathbf{C}_j + 2\Lambda_j - (\mathbf{L}_{j-1} + m_{j-1})^2 \Lambda_{j-1} \mathbf{C}_{j-1} \mathbf{D}_{j-1}^{-1} \mathbf{C}_{j-1}^\top \Lambda_{j-1}, \quad (3)$$

where the triangular terms are represented as,

Lemma 4 *The block triangular terms of \mathbf{L}_{ij} for $j = \{1, \dots, n-1\}$, where $\mathbf{L}_{jj} = \mathbf{I}$, are the following,*

$$\mathbf{L}_{(j+1)j} = -(\mathbf{L}_j + m_j) \Lambda_j \mathbf{C}_j \mathbf{D}_j^{-1}, \quad (4)$$

$$\mathbf{L}_{(j+2)j} = \mathbf{0},$$

$$\vdots$$

$$\mathbf{L}_{nj} = \mathbf{0},$$

$$\mathbf{L}_{(n+1)j} = -\mathbf{J}_j \mathbf{D}_j^{-1}, \quad (5)$$

where we define \mathbf{J}_j as the following:

$$\mathbf{J}_j = \underbrace{\left[\prod_{k=1}^{j-1} (\mathbf{L}_k + m_k) \right]}_{\Upsilon_j} \mathbf{B}^\top \mathbf{A} \underbrace{\left[\prod_{k=1}^{j-1} \mathbf{D}_k^{-1} \mathbf{C}_k^\top \Lambda_k \right]}_{\Gamma_j}.$$

Lemma 5 *The last triangular off diagonal component not explicitly stated is $\mathbf{L}_{(n+1)n}$, which is defined as,*

$$\mathbf{L}_{(n+1)n} = -\mathbf{J}_n \mathbf{D}_n^{-1} - (L_n + m_n) \Lambda_n C_n \mathbf{D}_n^{-1}.$$

Finally the last block for the decomposition \mathbf{D}_{n+1} is defined as such,

Lemma 6 *The symmetric block diagonal \mathbf{D}_{n+1} is of the form,*

$$\mathbf{D}_{n+1} = 2\Lambda_n - B^\top B - B^\top A \left[\sum_{j=1}^n \Upsilon_j^2 \Gamma_j \mathbf{D}_j^{-1} \Gamma_j^\top \right] A^\top B - (L_n + m_n)^2 \Lambda_n C_n \mathbf{D}_n^{-1} C_n^\top \Lambda_n,$$

Proof Let M denote the symmetric matrix appearing in (2) (annotated as \bar{M}), which we negate to achieve the positive definite constraint, $M = -\bar{M}$. Thus the block entries of M (indexed $1, \dots, n+1$) are the negated blocks of (2). We seek an LDL^\top factorization

$$M = \mathbf{L} \mathbf{D} \mathbf{L}^\top,$$

where \mathbf{L} is block unit lower-triangular ($\mathbf{L}_{jj} = \mathbf{I}$) and $\mathbf{D} = \text{diag}(\mathbf{D}_1, \dots, \mathbf{D}_{n+1})$ is block diagonal. We prove by induction on j that the block diagonal factors \mathbf{D}_j and the nonzero sub-diagonal blocks \mathbf{L}_{ij} satisfy the formulas given in Lemmas 2–6.

Base case ($j = 1$). We start by recalling the standard recursive relations from Theorem 1. Applying (LD1) returns,

$$\mathbf{D}_1 = M_{11}.$$

where M_{11} from (2) outputs,

$$\mathbf{D}_1 = \mathcal{L}^2 \mathbf{I} + 2L_1 m_1 C_1^\top \Lambda_1 C_1 - A^\top A,$$

which matches Lemma 2.

For the first column of \mathbf{L} -blocks, we use (LD2) with $j = 1$ from which we obtain that,

$$\mathbf{L}_{21} = M_{21} \mathbf{D}_1^{-1}.$$

Since $M_{21} = -(L_1 + m_1) \Lambda_1 C_1$, we have

$$\mathbf{L}_{21} = -(L_1 + m_1) \Lambda_1 C_1 \mathbf{D}_1^{-1},$$

which is the stated formula for $\mathbf{L}_{(1+1)1}$ from (4). For $i = \{3, \dots, n\}$ the matrix $M_{i1} = \mathbf{0}$, thus $\mathbf{L}_{i1} = \mathbf{0}$. Finally $M_{(n+1),1} = -B^\top A$, so

$$\mathbf{L}_{(n+1),1} = -B^\top A \mathbf{D}_1^{-1}.$$

Defining the empty products, $\Upsilon_1 := 1$ and $\Gamma_1 := \mathbf{I}$, we note $\mathbf{J}_1 = \Upsilon_1 B^\top A \Gamma_1 = B^\top A$, so $\mathbf{L}_{(n+1),1} = -\mathbf{J}_1 \mathbf{D}_1^{-1}$ as claimed in (5). This completes the base case.

Inductive hypothesis. Fix j with $1 \leq j \leq n$. Assume for all k with $1 \leq k \leq j$ the diagonal blocks \mathbf{D}_k and the nonzero sub-diagonal blocks \mathbf{L}_{ik} (for $i > k$) satisfy the Lemmas 2—6: We will prove the same pattern holds at index $j+1$ (for $j+1 \leq n+1$).

Inductive step: diagonal block \mathbf{D}_{j+1} for $1 \leq j < n$. Apply (LD1) with index $j+1$:

$$\mathbf{D}_{j+1} = M_{j+1,j+1} - \sum_{k=1}^j \mathbf{L}_{j+1,k} \mathbf{D}_k \mathbf{L}_{j+1,k}^\top.$$

From (2) we read

$$M_{j+1,j+1} = 2L_{j+1}m_{j+1}C_{j+1}^\top\Lambda_{j+1}C_{j+1} + 2\Lambda_j.$$

Due to the sparsity of M and the inductive hypothesis, the only nonzero $\mathbf{L}_{j+1,k}$ with $1 \leq k \leq j$ is $\mathbf{L}_{j+1,j} = -(L_j + m_j)\Lambda_j C_j \mathbf{D}_j^{-1}$. Which reduces the system to,

$$\mathbf{L}_{j+1,j} \mathbf{D}_j \mathbf{L}_{j+1,j}^\top = (L_j + m_j)^2 \Lambda_j C_j \mathbf{D}_j^{-1} C_j^\top \Lambda_j.$$

Thus,

$$\mathbf{D}_{j+1} = 2L_{j+1}m_j C_{j+1}^\top \Lambda_{j+1} C_{j+1} + 2\Lambda_{j+1} - (L_j + m_j)^2 \Lambda_j C_j \mathbf{D}_j^{-1} C_j^\top \Lambda_j,$$

which matches Lemma 3 (with index shift $j \mapsto j+1$).

Inductive step: sub-diagonal blocks in column $j+1$. Use (LD2):

$$\mathbf{L}_{i,j+1} = \left(M_{i,j+1} - \sum_{k=1}^j \mathbf{L}_{ik} \mathbf{D}_k \mathbf{L}_{j+1,k}^\top \right) \mathbf{D}_{j+1}^{-1}, \quad i > j+1.$$

For $i = \{j+3, \dots, n\}$ we have $M_{i,j+1} = \mathbf{0}$ and by the inductive hypothesis $\mathbf{L}_{ik} = \mathbf{0}$ for all $k \leq j$; hence the internal components vanishes and $\mathbf{L}_{i,j+1} = \mathbf{0}$ for $i = \{j+3, \dots, n\}$.

For the last row $i = n+1$ we calculate,

$$\mathbf{L}_{(n+1),j+1} = \left(M_{(n+1),j+1} - \sum_{k=1}^j \mathbf{L}_{(n+1),k} \mathbf{D}_k \mathbf{L}_{j+1,k}^\top \right) \mathbf{D}_{j+1}^{-1}.$$

By the inductive hypothesis $\mathbf{L}_{(n+1),k} = -\mathbf{J}_k \mathbf{D}_k^{-1}$ for $k \leq j$, and the only nonzero $\mathbf{L}_{j+1,k}$ with $k \leq j$ is $\mathbf{L}_{j+1,j} = -(L_j + m_j)\Lambda_j C_j \mathbf{D}_j^{-1}$. Therefore, the summation reduces,

$$\begin{aligned} \mathbf{L}_{(n+1),j} \mathbf{D}_j \mathbf{L}_{j+1,j}^\top &= (-\mathbf{J}_j \mathbf{D}_j^{-1}) \mathbf{D}_j (-(L_j + m_j)\Lambda_j C_j \mathbf{D}_j^{-1})^\top \\ &= \mathbf{J}_j \mathbf{D}_j^{-1} (L_j + m_j)\Lambda_j C_j^\top \Lambda_j. \end{aligned}$$

Substituting $M_{(n+1),j+1}$ from (2),

$$\mathbf{L}_{(n+1),j+1} = -\mathbf{J}_{j+1} \mathbf{D}_{j+1}^{-1},$$

which is exactly the formula claimed in (5).

The immediate sub-diagonal $\mathbf{L}_{(j+1),j}$ is obtained directly from (LD2) at step j :

$$\mathbf{L}_{(j+1),j} = M_{(j+1),j} \mathbf{D}_j^{-1} = -(L_j + m_j) \Lambda_j C_j \mathbf{D}_j^{-1}.$$

Final diagonal block \mathbf{D}_{n+1} . Applying (LD1) at $j = n + 1$ returns:

$$\mathbf{D}_{n+1} = M_{n+1,n+1} - \sum_{k=1}^n \mathbf{L}_{n+1,k} \mathbf{D}_k \mathbf{L}_{n+1,k}^\top.$$

From (2) we have $M_{n+1,n+1} = 2\Lambda_n - B^\top B$ and using the inductive results from above, we derive that,

$$\begin{aligned} \mathbf{L}_{n+1,k} &= -\mathbf{J}_k \mathbf{D}_k^{-1} \quad (k = 1, \dots, n-1), \\ \mathbf{L}_{n+1,n} &= -\mathbf{J}_n \mathbf{D}_n^{-1} - (L_n + m_n) \Lambda_n C_n \mathbf{D}_n^{-1}, \end{aligned}$$

and telescoping the summation, while canceling \mathbf{D}_k with \mathbf{D}_k^{-1} , produces the closed form,

$$\begin{aligned} \mathbf{D}_{n+1} &= 2\Lambda_n - B^\top B - \mathbf{L}_{(n+1)1} \mathbf{D}_1 \mathbf{L}_{(n+1)1}^\top - \mathbf{L}_{(n+1)2} \mathbf{D}_2 \mathbf{L}_{(n+1)2}^\top - \dots - \mathbf{L}_{(n+1)n} \mathbf{D}_n \mathbf{L}_{(n+1)n}^\top, \\ &= 2\Lambda_n - B^\top B - \left(\sum_{j=1}^n \mathbf{J}_j \mathbf{D}_j^{-1} \mathbf{J}_j^\top + (L_n + m_n)^2 \Lambda_n C_n \mathbf{D}_n^{-1} C_n^\top \Lambda_n \right), \\ &= 2\Lambda_n - B^\top B - B^\top A \left[\sum_{j=1}^n \Upsilon_j^2 \Gamma_j \mathbf{D}_j^{-1} \Gamma_j^\top \right] A^\top B - (L_n + m_n)^2 \Lambda_n C_n \mathbf{D}_n^{-1} C_n^\top \Lambda_n, \\ \mathbf{D}_{n+1} &= 2\Lambda_n - B^\top B - B^\top A \left[\sum_{j=1}^n \Upsilon_j^2 \Gamma_j \mathbf{D}_j^{-1} \Gamma_j^\top \right] A^\top B - (L_n + m_n)^2 \Lambda_n C_n \mathbf{D}_n^{-1} C_n^\top \Lambda_n, \end{aligned}$$

This matches the final Lemma 6.

Conclusion. We have shown the base case, where $j = 1$, and proved by induction that if the asserted formulas are valid up to index j then they must hold at index $j + 1$. By induction, the formulas for \mathbf{D}_1 , \mathbf{D}_j , for $j = \{2, \dots, n\}$, \mathbf{D}_{n+1} , and for the nonzero block-sub-diagonal entries of \mathbf{L} hold for all the necessary indices. This thus completes the proof. ■

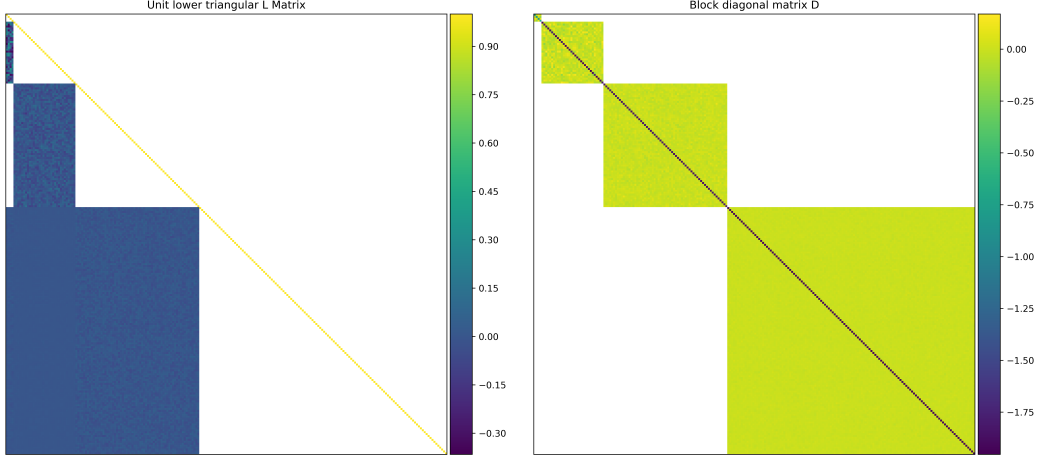
Given the new structure, we can see the sparsity of the system decomposition resulting in the initial sparsity of the general LMI with $\mathbf{L}_{(j+2)j} = \dots = \mathbf{L}_{nj} = \mathbf{0}$, which significantly reduces the diagonal components' complexities to constrain each of the parameters in the system.

The following properties are demonstrated empirically with the unit triangular matrix \mathbf{L} structure in Figure 1a and the block diagonal matrix \mathbf{D} illustrated in Figure 1b.

3.2 Constraints

Given Table 7 in Appendix A, the majority (56%) of the activation function have the property that $P = 0$ and $S = 1$, for the continuation of this derivation we will assume that $L_i = 1$ and $m_j = 0$, which thus generates the following symmetric block diagonals,

$$\mathbf{D}_1 = \mathcal{L}^2 \mathbf{I} - A^\top A,$$



(a) Unit lower-triangular factor \mathbf{L} (unitriangular), showing the sparsity pattern implied by the LDL^\top block factorization of matches the closed forms in Lemmas 2–6 the negated LMI $M = -\bar{M}$; in particular, and satisfies $\mathbf{D}_i \succeq \mathbf{0}$ under the imposed constraints.

Figure 1: Structure of the factors in the block LDL^\top decomposition used to certify positive semidefiniteness of the LMI. Visualizations are generated from a randomly initialized LDL^\top network with input/output dimension 4 and hidden layer widths [32, 64, 256, 256].

$$\begin{aligned} \mathbf{D}_j &= 2\Lambda_j - \Lambda_{j-1}C_{j-1}\mathbf{D}_{j-1}^{-1}C_{j-1}^\top\Lambda_{j-1}, \quad \forall j \in \{2, \dots, n\}, \\ \mathbf{D}_{n+1} &= 2\Lambda_n - B^\top \left(\mathbf{I} + A \left[\sum_{j=1}^n \Gamma_j \mathbf{D}_j^{-1} \Gamma_j^\top \right] A^\top \right) B - \Lambda_n C_n \mathbf{D}_n^{-1} C_n^\top \Lambda_n, \end{aligned}$$

for which, the following conditions are imposed on the matrices $\mathbf{D}_j \succeq \mathbf{0}, \forall i \in \{1, \dots, n+1\}$ by finding the parameterization of $A, B, \{C_j, \Lambda_j\}_{j=1:n}$ such that the desired constraints are satisfied.

Lemma 7 *The matrix A needs to be constrained such that,*

$$\|A\|_2 \leq \mathcal{L},$$

Proof Beginning with the first block,

$$\mathbf{D}_1 = \mathcal{L}^2 \mathbf{I} - A^\top A \succeq 0.$$

which can thus be manipulated such that,

$$A^\top A \preceq \mathcal{L}^2 \mathbf{I}, \tag{6}$$

Given that $\|M\|_2$ represents the spectral norm, defined $\|M\|_2 = \sqrt{\lambda_{\max}(M^\top M)}$, we have,

$$\begin{aligned}\lambda_{\max}(A^\top A) &\leq \mathcal{L}^2, \\ \sqrt{\lambda_{\max}(A^\top A)} &\leq \mathcal{L}, \\ \|A\|_2 &\leq \mathcal{L}.\end{aligned}$$

■

Based on the intermediary block \mathbf{D}_j for $j \in \{2, n\}$ we have that,

Lemma 8 *The matrices $\{C_j, \Lambda_j\}_{j=1:n-1}$ need to be constrained such that,*

$$\left\| C_j \mathbf{D}_j^{-\frac{1}{2}} \right\|_2 \leq \sqrt{2}, \quad \forall j \in \{1, \dots, n-1\},$$

with $\{\Lambda_j\}_{j=1:n-1} = \mathbf{I}$

Proof Starting with the intermediary block definition for $j \in \{2, n\}$,

$$\mathbf{D}_j = 2\Lambda_j - \Lambda_{j-1} C_{j-1} \mathbf{D}_{j-1}^{-1} C_{j-1}^\top \Lambda_{j-1} \succeq \mathbf{0},$$

we thus get the requirement that,

$$\Lambda_{j-1} C_{j-1} \mathbf{D}_{j-1}^{-1} C_{j-1}^\top \Lambda_{j-1} \preceq 2\Lambda_j,$$

where a simple solution can be derived if $\Lambda_{j-1} = \mathbf{I}$,

$$\begin{aligned}C_{j-1} \mathbf{D}_{j-1}^{-1} C_{j-1}^\top &\preceq 2\mathbf{I}, \\ \left(C_{j-1} \mathbf{D}_{j-1}^{-\frac{1}{2}} \right) \left(\mathbf{D}_{j-1}^{-\frac{1}{2}} C_{j-1}^\top \right) &\preceq 2\mathbf{I},\end{aligned}\tag{7}$$

where by the same argument in the proof 3.2, the spectral norm is thus constructed. We can take the inverse square root of \mathbf{D}_{j-1} , as we know by induction that $\mathbf{D}_{j-1} \succ \mathbf{0}$, which means that $\mathbf{D}_{j-1}^{-1} \succ \mathbf{0}$, which then means that there exists a square root of the matrix. ■

The last two constraints that need to be obtained are the parameters $\{C_n, \Lambda_n\}$ and B , which can both be obtained through the last block \mathbf{D}_{n+1} ,

Lemma 9 *The matrix C_n has to be constrained such that,*

$$\left\| C_n \mathbf{D}_n^{-\frac{1}{2}} \right\|_2 \leq \sqrt{2},$$

where $\Lambda_n = \mathbf{I}$ and B needs to be constrained such that,

$$\left\| \left(\mathbf{I} + A \Sigma A^\top \right)^{1/2} B \right\|_2 \leq \sqrt{\|2\mathbf{I} - C_n \mathbf{D}_n^{-1} C_n^\top\|_2}.$$

Proof Starting with the last block \mathbf{D}_{n+1} 's definition,

$$\mathbf{D}_{n+1} = 2\Lambda_n - B^\top \left(\mathbf{I} + A \left[\sum_{j=1}^n \Gamma_j \mathbf{D}_j^{-1} \Gamma_j^\top \right] A^\top \right) B - \Lambda_n C_n \mathbf{D}_n^{-1} C_n^\top \Lambda_n,$$

we set $\Lambda_n = \mathbf{I}$ resulting in,

$$\mathbf{D}_{n+1} = 2\mathbf{I} - B^\top \left(\mathbf{I} + A \left[\sum_{j=1}^n \Gamma_j \mathbf{D}_j^{-1} \Gamma_j^\top \right] A^\top \right) B - C_n \mathbf{D}_n^{-1} C_n^\top,$$

we know by definition that all previous $\mathbf{D}_j \succeq \mathbf{0}$ for $j \in \{1, \dots, n\}$ based on the constraints defined in the lemmas above, as such $\mathbf{D}_j^{-1} \succeq \mathbf{0}$ for $j \in \{1, \dots, n\}$, which in turn means that $\Gamma_j \mathbf{D}_j^{-1} \Gamma_j^\top \succeq \mathbf{0}$. and thus, $\Sigma = \sum_{j=1}^n \Gamma_j \mathbf{D}_j^{-1} \Gamma_j^\top \succeq \mathbf{0}$. Thus,

$$B^\top \left(\mathbf{I} + A \Sigma A^\top \right) B \preceq 2\mathbf{I} - C_n \mathbf{D}_n^{-1} C_n^\top.$$

Given that $B^\top \left(\mathbf{I} + A \Sigma A^\top \right) B \succeq \mathbf{0}$ this means that we need that $2\mathbf{I} - C_n \mathbf{D}_n^{-1} C_n^\top \succeq \mathbf{0}$ to provide a valid solution. As such

$$2\mathbf{I} - C_n \mathbf{D}_n^{-1} C_n^\top \succeq \mathbf{0}, \quad (8)$$

which is symmetric and diagonalizable, which returns the constraints that

$$\left\| C_n \mathbf{D}_n^{-\frac{1}{2}} \right\|_2 \leq \sqrt{2}, \quad (9)$$

which results in

$$\begin{aligned} B^\top \left(\mathbf{I} + A \Sigma A^\top \right) B &\preceq 2\mathbf{I} - C_n \mathbf{D}_n^{-1} C_n^\top, \\ \left[B^\top \left(\mathbf{I} + A \Sigma A^\top \right)^{-\frac{1}{2}} \right] \left[\left(\mathbf{I} + A \Sigma A^\top \right)^{-\frac{1}{2}} B \right] &\preceq M, \\ \left\| B^\top \left(\mathbf{I} + A \Sigma A^\top \right)^{1/2} \right\|_2 &\leq \sqrt{\|M\|_2}. \end{aligned} \quad (10)$$

Theorem 10 *The spectral norm is invariant to the transpose, $\|A^\top A\|_2 = \|A A^\top\|_2 = \|A\|_2^2$.*

thus, applying it to the constraint yields the final constraint. ■

The parameterization of B can further be tightened in the following manner,

Lemma 11 *For the matrix B and the positive definite symmetric matrices C and D , the constraint*

$$B^\top C B \preceq D,$$

can be constrained as,

$$B = C^{-\frac{1}{2}} W_B (\alpha_B \mathbf{I} + W_B^\top W_B)^{-\frac{1}{2}} D^{\frac{1}{2}},$$

Proof

$$\begin{aligned}
 B^\top CB &= D^{\frac{1}{2}}(\alpha_B \mathbf{I} + W_B^\top W_B)^{-\frac{1}{2}} W_B^\top C^{-\frac{1}{2}} C C^{-\frac{1}{2}} W_B (\alpha_B \mathbf{I} + W_B^\top W_B)^{-\frac{1}{2}} D^{\frac{1}{2}}, \\
 &= D^{\frac{1}{2}}(\alpha_B \mathbf{I} + W_B^\top W_B)^{-\frac{1}{2}} W_B^\top W_B (\alpha_B \mathbf{I} + W_B^\top W_B)^{-\frac{1}{2}} D^{\frac{1}{2}}, \\
 &\preceq D^{\frac{1}{2}} \mathbf{I} D^{\frac{1}{2}} \preceq D.
 \end{aligned} \tag{11}$$

■

this means that the most accurate constraint for the system,

$$B = \left(\mathbf{I} + A \Sigma A^\top \right)^{-1/2} W_B (\alpha_B \mathbf{I} + W_B^\top W_B)^{-\frac{1}{2}} \left(2\mathbf{I} - C_n \mathbf{D}_n^{-1} C_n^\top \right)^{\frac{1}{2}}. \tag{12}$$

3.3 Variable Parameterization

Now that each variable has constraints imposed on it, it is necessary to find a parameterization for each variable to ensure that each constraint is satisfied.

Lemma 12 *If a matrix is parameterized as,*

$$M = \gamma W (\alpha \mathbf{I} + W^\top W)^{-\frac{1}{2}},$$

for any $W \in \mathbb{R}^{\dim(M)}$, and $\gamma, \alpha > 0$ (can be parameterized using $\gamma = e^{\tilde{\gamma}}, \tilde{\gamma} \in \mathbb{R}$). Then $\|M\|_2 \leq \gamma$

Proof Given the matrix M parameterized as stated above,

$$\begin{aligned}
 M^\top M &= \gamma^2 (\alpha \mathbf{I} + W^\top W)^{-\frac{1}{2}} W^\top W (\alpha \mathbf{I} + W^\top W)^{-\frac{1}{2}}, \\
 &= \gamma^2 (\alpha \mathbf{I} + A)^{-\frac{1}{2}} A (\alpha \mathbf{I} + A)^{-\frac{1}{2}},
 \end{aligned}$$

where $A = W^\top W \succeq \mathbf{0}$. Since A is a positive definitive matrix there exists an orthogonal matrix Q ($Q^\top Q = \mathbf{I}$) and a diagonal matrix $\Lambda = \text{diag}(\mu_1, \dots, \mu_n)$ with $\mu_i \geq 0$ such that $A = Q \Lambda Q^\top$,

$$\begin{aligned}
 M^\top M &= \gamma^2 (\alpha \mathbf{I} + A)^{-\frac{1}{2}} A (\alpha \mathbf{I} + A)^{-\frac{1}{2}}, \\
 &= \gamma^2 Q (\alpha \mathbf{I} + \Lambda)^{-\frac{1}{2}} Q^\top (Q \Lambda Q^\top) Q (\alpha \mathbf{I} + \Lambda)^{-\frac{1}{2}} Q^\top, \\
 &= \gamma^2 Q (\alpha \mathbf{I} + \Lambda)^{-\frac{1}{2}} \Lambda (\alpha \mathbf{I} + \Lambda)^{-\frac{1}{2}} Q^\top, \\
 &= \gamma^2 Q \text{diag} \left(\frac{\mu_1}{\alpha + \mu_1}, \dots, \frac{\mu_n}{\alpha + \mu_n} \right) Q^\top,
 \end{aligned}$$

where $\frac{\mu_i}{\alpha + \mu_i} < 1$. As such $\|M\|_2^2 = \max_i \frac{\mu_i}{\alpha + \mu_i}$. Since the largest μ_i is $\mu_{\max} = \|W\|_2^2$.

In turn:

$$\begin{aligned}
 \|M\|_2^2 &= \gamma^2 \frac{\mu_{\max}}{\alpha + \mu_{\max}} = \gamma^2 \frac{\|W\|_2^2}{\alpha + \|W\|_2^2}, \\
 \|M\|_2 &= \gamma \frac{\|W\|_2}{\sqrt{\alpha + \|W\|_2^2}} \leq \gamma.
 \end{aligned}$$

■

Based on the parameterization in Lemma 12, the parameterization of A is derived as,

$$A = \mathcal{L}W_A(\alpha_A \mathbf{I} + W_A^\top W_A)^{-\frac{1}{2}}, \quad (\text{PA})$$

where $W_A \in \mathbb{R}^{\dim A}$, which guarantees the condition imposed in Lemma 7. Similarly, $\{C_j\}_{j=1:n}$ are constructed as,

$$C_j = \sqrt{2}W_j(\alpha_j \mathbf{I} + W_j^\top W_j)^{-\frac{1}{2}} \mathbf{D}_j^{\frac{1}{2}}, \quad \forall j \in \{1, \dots, n\}, \quad (\text{PC})$$

where $W_j \in \mathbb{R}^{\dim C_j}$, $\forall j \in \{1, \dots, n\}$ which also satisfies the constraints constructed in Lemma 8 and 9. The final parameter B can be parameterized as,

$$B = \left(\mathbf{I} + A \Sigma A^\top \right)^{-1/2} W_B (\alpha_B \mathbf{I} + W_B^\top W_B)^{-\frac{1}{2}} \left(2\mathbf{I} - C_n \mathbf{D}_n^{-1} C_n^\top \right)^{\frac{1}{2}}, \quad (13)$$

where $W_B \in \mathbb{R}^{\dim B}$, which guarantees the conditions in Lemma 9. The recursive dependence on \mathbf{D}_j , necessitates an eigen-decomposition of the matrix \mathbf{D}_j , to compute the matrix square root. Both of these points will be addressed in Section 4.1. This parameterization is closely related to spectral normalization (Miyato et al., 2018), and to a norm-based Lipschitz regularization (Gouk et al., 2021), but yields an exact spectral-norm bound rather than relying on power iteration or layer-wise upper bounds, acting closer to the orthonormal Cayley transform parameterization from Wang and Manchester (2023).

3.4 Diagonal Block Simplifications

Given the new parameterizations of the parameters $A, B, \{C_j\}_{j=1:n}$, we can now derive simplifications for the blocks $\{D_j\}_{j=1:n+1}$. Starting with D_1 , we have that,

Lemma 13 *The simplification of D_1 is*

$$D_1 = \mathcal{L}^2 \alpha_A (\alpha_A \mathbf{I} + W_A^\top W_A)^{-1}.$$

Proof We start with the initial definition of D_1 , Lemma 2, and A , defined in Equation (PA),

$$\begin{aligned} D_1 &= \mathcal{L}^2 \mathbf{I} - A^\top A, \\ &= \mathcal{L}^2 \mathbf{I} - \mathcal{L}^2 (\alpha_A \mathbf{I} + W_A^\top W_A)^{-\frac{1}{2}} W_A^\top W_A (\alpha_A \mathbf{I} + W_A^\top W_A)^{-\frac{1}{2}}, \\ &= \mathcal{L}^2 \left(\mathbf{I} - (\alpha_A \mathbf{I} + M)^{-\frac{1}{2}} M (\alpha_A \mathbf{I} + M)^{-\frac{1}{2}} \right), \end{aligned}$$

substituting $M = (\alpha_A \mathbf{I} + M) - \alpha_A \mathbf{I}$, where $M = W_A^\top W_A$ and $V = (\alpha_A \mathbf{I} + M)$,

$$\begin{aligned} D_1 &= \mathcal{L}^2 \left(\mathbf{I} - V^{-\frac{1}{2}} (V - \alpha_A \mathbf{I}) V^{-\frac{1}{2}} \right), \\ &= \mathcal{L}^2 \left(\mathbf{I} - \mathbf{I} + \alpha_A V^{-1} \right), \\ &= \mathcal{L}^2 \alpha_A (\alpha_A \mathbf{I} + M)^{-1} = \mathcal{L}^2 \alpha_A \left(\alpha_A \mathbf{I} + W_A^\top W_A \right)^{-1}. \end{aligned}$$

■

The $\{D_j\}_{j=2:n}$ can also be simplified using,

Theorem 14 *The Woodbury matrix identity (Woodbury, 1950), otherwise called the matrix inversion lemma, states that*

$$(A + UCV)^{-1} = A^{-1} - A^{-1}U(C^{-1} + VA^{-1}U)^{-1}VA^{-1},$$

where $A \in \mathbb{R}^{n \times n}$, $U \in \mathbb{R}^{n \times k}$, $C \in \mathbb{R}^{k \times k}$ and $V \in \mathbb{R}^{k \times n}$ and A is invertible.

Corollary 15 *The following matrix inverses are equivalent*

$$\alpha(\alpha \mathbf{I} + MM^\top)^{-1} = \mathbf{I} - M(\alpha \mathbf{I} + M^\top M)^{-1}M^\top,$$

given through the Woodbury matrix identity in Theorem 14. By setting $A = \alpha \mathbf{I}$, $C = \frac{1}{\alpha} \mathbf{I}$, $U = \sqrt{\alpha}M$ and $V = \sqrt{\alpha}M^\top$

which allows for the follow simplifications of $\{D_j\}_{j=2:n}$,

Lemma 16 *For $j = \{2, \dots, n\}$, D_j can be simplified to be,*

$$D_j = 2\alpha_{j-1}(\alpha_{j-1}\mathbf{I} + W_{j-1}W_{j-1}^\top)^{-1}, \quad \forall j \in \{2, \dots, n\}.$$

Proof Starting with the general definitions of $\{D_j\}_{j=2:n}$, Lemma 3, and $\{C_j\}_{j=1:n}$, defined in Equation (PC), we have that $V_j = \alpha_j \mathbf{I} + W_j^\top W_j$,

$$\begin{aligned} D_j &= 2\mathbf{I} - C_{j-1}D_{j-1}^{-1}C_{j-1}^\top, \quad \forall j \in \{2, \dots, n\}, \\ &= 2\mathbf{I} - 2W_{j-1}V^{-\frac{1}{2}}D_{j-1}^{\frac{1}{2}}D_{j-1}^{-1}D_{j-1}^{\frac{1}{2}}V^{-\frac{1}{2}}W_{j-1}^\top, \\ &= 2\left(\mathbf{I} - W_{j-1}(\alpha_{j-1}\mathbf{I} + W_{j-1}^\top W_{j-1})^{-1}W_{j-1}^\top\right). \end{aligned}$$

Using Corollary 15 with $A = W_{j-1}$ we thus have that,

$$D_j = 2\alpha_{j-1}(\alpha_{j-1}\mathbf{I} + W_{j-1}W_{j-1}^\top)^{-1}, \quad \forall j \in \{2, \dots, n\}.$$

■

Which thus simplifies the $\{C_j\}_{j=1:n}$ to,

$$\begin{aligned} C_1 &= \mathcal{L}\sqrt{2\alpha_A}W_1\Omega_1^{-\frac{1}{2}}\Omega_0^{-\frac{1}{2}}, \\ C_j &= 2\sqrt{\alpha_{j-1}}W_j\Omega_j^{-\frac{1}{2}}\Omega_{j-1}^{-\frac{1}{2}}, \quad \forall j \in \{2, \dots, n\}, \end{aligned}$$

with,

$$\Omega_j = \begin{cases} \alpha_A \mathbf{I} + W_A^\top W_A, & \text{if } j = 0 \\ \alpha_j \mathbf{I} + W_j W_j^\top, & \text{else} \end{cases}.$$

3.5 B Expansion

Based on the previous definition of B in Equation (13) as,

$$B = \left(\mathbf{I} + A\Sigma A^\top\right)^{-1/2} W_B(\alpha_B \mathbf{I} + W_B^\top W_B)^{-\frac{1}{2}} \left(2\mathbf{I} - C_n D_n^{-1} C_n^\top\right)^{\frac{1}{2}},$$

there are specific components that can be simplified in this system,

3.5.1 RECURSIVE NORMALIZER

The recursive normalization constant, $(\mathbf{I} + A\Sigma A^\top)^{-1/2}$ needs to be expanded to be further understood now that interior components have been fully defined. The most important component in the system is the $A\Sigma A^\top$. We have,

$$\Sigma = \sum_{j=1}^n \Gamma_j \mathbf{D}_j^{-1} \Gamma_j^\top, \quad \Gamma_j = \prod_{k=1}^{j-1} \mathbf{D}_k^{-1} C_k^\top,$$

which is very computationally inexpensive to compute when viewed as an iterative process. From the product form of Γ_j , we obtain the simple recurrence

$$\Gamma_1 = \mathbf{I}, \quad (14)$$

$$\Gamma_{j+1} = \Gamma_j \mathbf{D}_j^{-1} C_j^\top, \quad j \geq 1. \quad (15)$$

which allows Σ to be computed efficiently though Algorithm 1, especially since if $\{C_j\}_{j=1:n}$ have been computed, the derivation of \mathbf{D}_j^{-1} is trivial since it equivalent to $c\Omega_{j-1}$, $c > 0$, which is much more computationally efficient than having to take the inverse of the matrices. we can simplify and expand the system to (setting all $\alpha = 1$),

Algorithm 1 Iterative Σ update

Input: matrices $\{\mathbf{D}_j, C_j\}_{j=1}^n$ (each \mathbf{D}_j invertible)

Initialize: $\Gamma_1 \leftarrow \mathbf{I}$, $\Sigma \leftarrow \mathbf{0}$

for $j = 1 \dots n$ **do**

$T \leftarrow \Gamma_j \mathbf{D}_j^{-1}$

▷ compute once and reuse

$\Sigma \leftarrow \Sigma + T\Gamma_j^\top$

▷ since $T\Gamma_j^\top = \Gamma_j \mathbf{D}_j^{-1} \Gamma_j^\top$

$\Gamma_{j+1} \leftarrow TC_j^\top$

▷ update to Γ_{j+1}

end for

Output: Σ

$$\begin{aligned} \Gamma_j &= \prod_{k=1}^{j-1} \mathbf{D}_k^{-1} C_k^\top = \prod_{k=1}^{j-1} \sqrt{2} \mathbf{D}_k^{-1} \mathbf{D}_k^{\frac{1}{2}} (\mathbf{I} + W_k^\top W_k)^{-\frac{1}{2}} W_k^\top = 2^{\frac{j-1}{2}} \prod_{k=1}^{j-1} \mathbf{D}_k^{-\frac{1}{2}} (\mathbf{I} + W_k^\top W_k)^{-\frac{1}{2}} W_k^\top, \\ &= 2^{\frac{j-1}{2}} \prod_{k=1}^{j-1} \left(\begin{cases} \mathcal{L}^2 & k = 1 \\ 2 & \text{else} \end{cases} \Omega_{k-1}^{-1} \right)^{-\frac{1}{2}} (\mathbf{I} + W_k^\top W_k)^{-\frac{1}{2}} W_k^\top, \\ &= 2^{\frac{j-1}{2}} \prod_{k=1}^{j-1} \begin{cases} \mathcal{L}^{-1} & k = 1 \\ 2^{-\frac{1}{2}} & \text{else} \end{cases} \Omega_{k-1}^{\frac{1}{2}} \Omega_k^{-\frac{1}{2}} W_k^\top, \\ &= \begin{cases} 1 & j = 1 \\ 2^{\frac{j-1}{2}} 2^{-\frac{j-2}{2}} \mathcal{L}^{-1} & \text{else} \end{cases} \prod_{k=1}^{j-1} \Omega_{k-1}^{\frac{1}{2}} \Omega_k^{-\frac{1}{2}} W_k^\top, \\ &= \begin{cases} 1 & j = 1 \\ \frac{\sqrt{2}}{\mathcal{L}} & \text{else} \end{cases} \underbrace{\prod_{k=1}^{j-1} \Omega_{k-1}^{\frac{1}{2}} \Omega_k^{-\frac{1}{2}} W_k^\top}_{\Xi_j}, \end{aligned} \quad (16)$$

with,

$$\begin{aligned}
 \Sigma &= \sum_{j=1}^n \Gamma_j \mathbf{D}_j^{-1} \Gamma_j^\top, \\
 &= \sum_{j=1}^n \Gamma_j \left(\begin{cases} \mathcal{L}^2 & j = 1 \\ 2 & \text{else} \end{cases} \Omega_{j-1}^{-1} \right)^{-1} \Gamma_j^\top, \\
 &= \sum_{j=1}^n \left(\begin{cases} \mathcal{L}^{-2} & j = 1 \\ 2^{-1} & \text{else} \end{cases} \right) \Gamma_j \Omega_{j-1} \Gamma_j^\top, \\
 &= \sum_{j=1}^n \left(\begin{cases} \mathcal{L}^{-2} \times 1 & j = 1 \\ 2^{-1} \times \frac{2}{\mathcal{L}^2} & \text{else} \end{cases} \right) \Xi_j \Omega_{j-1} \Xi_j^\top, \\
 &= \mathcal{L}^{-2} \sum_{j=1}^n \Xi_j \Omega_{j-1} \Xi_j^\top.
 \end{aligned}$$

The simplification of $A\Sigma A^\top$, helps further reduce the system,

$$\begin{aligned}
 A\Sigma A^\top &= \mathcal{L}^2 W_A \Omega_0^{-\frac{1}{2}} \Sigma (\Omega_0^{-\frac{1}{2}})^\top W_A^\top, \\
 &= W_A \Omega_0^{-\frac{1}{2}} \left(\sum_{j=1}^n \Xi_j \Omega_{j-1} \Xi_j^\top \right) (\Omega_0^{-\frac{1}{2}})^\top W_A^\top, \\
 &= W_A W_A^\top + W_A \Omega_0^{-\frac{1}{2}} \left(\sum_{j=2}^n \Xi_j \Omega_{j-1} \Xi_j^\top \right) (\Omega_0^{-\frac{1}{2}})^\top W_A^\top.
 \end{aligned}$$

Again we have the computational complexity of the problem being dominated from $\Omega_{k-1}^{\frac{1}{2}}$ and $\Omega_k^{-\frac{1}{2}}$ inside Γ , however, as from Section 4.1, we can rewrite Ω_k by the decomposition,

$$\Omega_k = R_k^\top R_k,$$

which we already need to compute for the computational speedups, thus we have the very efficient computation of $\Omega_k^{\frac{1}{2}}$ simply as R_k^\top , and we would thus get equivalent singular value bounds,

Lemma 17 *Define $S =$ For every PSD matrix A , we define $S = A^{\frac{1}{2}}$ as the unique symmetric PSD square root matrix ($A = SS^\top = S^\top S$) and R the upper triangular Cholesky decomposition $A = R^\top R$. We state that there exists an orthogonal matrix Q such that,*

$$R^\top = SQ, \quad \text{equivalently} \quad S = R^\top Q^\top,$$

and

$$S^{-1} = QR^{-\top}, \quad S^{-1} = Q^\top R^{-\top},$$

depending on the chosen orientation for Q 's definition.

Proof Because $A = R^\top R = S^2$, the matrices R and S are two invertible square roots of the same PSD matrix, thus the product

$$Q = S^{-1}R^\top, \quad \text{or,} \quad Q = RS^{-1},$$

is well defined and thus satisfies,

$$QQ^\top = S^{-1}R^\top RS^{-1} = S^{-1}AS^{-1} = S^{-1}S^2S^{-1} = \mathbf{I}.$$

■

Proposition 18 *The factor $A\Sigma A^\top$ cannot be rewritten as the computationally optimized version,*

$$\begin{aligned} \bar{\Xi}_j &= \prod_{k=1}^{j-1} R_{k-1}^\top R_k^{-\top} W_k^\top, \\ \bar{A}\bar{\Sigma}\bar{A}^\top &= W_A W_A^\top + W_A R_A^{-1} \left(\sum_{j=2}^n \bar{\Xi}_j \Omega_{j-1} \bar{\Xi}_j^\top \right) R_A^{-\top} W_A^\top. \end{aligned} \quad (17)$$

Proof To verify that this reparameterization of the system is indeed correct, we need to ensure that the norm of the matrix is maintained, such that $\|A\Sigma A^\top\|_2 = \|\bar{A}\bar{\Sigma}\bar{A}^\top\|$ and is equivalent between the two formulation. We start with the symmetric formulation where $S_j^2 = \Omega_j$.

$$\begin{aligned} \Xi_j &= \prod_{k=1}^{j-1} S_{k-1} S_k^{-1} W_k^\top, \\ A\Sigma A^\top &= W_A W_A^\top + W_A S_A^{-1} \left(\sum_{j=2}^n \Xi_j \Omega_{j-1} \Xi_j^\top \right) S_A^{-\top} W_A^\top. \end{aligned}$$

now we replace each S with $S_j = R_j^\top Q_j^\top$ and $S_j^{-1} = Q_j^\top R_j^{-\top}$, we get that,

$$\begin{aligned} S_{k-1} S_j^{-1} &= (R_{j-1}^\top Q_{j-1}^\top)(Q_j^\top R_j^{-\top}), \\ &= R_{j-1}^\top (Q_{j-1}^\top Q_j) R_j^{-\top}, \end{aligned}$$

define the orthogonal factor,

$$\bar{Q}_j = Q_{j-1}^\top Q_j,$$

as such, it is improbable to have the decomposition be directly equal to each other such that the form proposed in Equation (17) is valid ($\bar{Q}_j = \mathbf{I}$ in that formulation). This would imply that $Q_{j-1} = Q_j$, which by induction thus imposes the constraint that $Q_1 = \dots = Q_n$. This would imply that $S_1 = \dots = S_n$, which is not possible unless all Ω_j equal each other. This, by sheer randomness, is improbable and, if strictly imposed, would cause a major reduction in expressiveness. ■

4 Computation Extensions

In this Section, we first describe how we can efficiently compute the square root of a matrix using Cholesky decomposition rather than a costly full eigenvalue decomposition. Following this we also briefly expand on how to implement the work to convolutional neural networks.

4.1 Square Root Computation

When tasked with deriving the square root of a matrix, the first thought is for a matrix to satisfy the following conditions,

Theorem 19 *If A is real symmetric positive semidefinite, then the square root, $A^{\frac{1}{2}}$, is used to denote the unique matrix B , that is positive semidefinite, and such that $BB = BB^T = A$ (Higham, 1986). There is precisely one square root B that is both positive semidefinite and symmetric (Horn and Johnson, 2012, Theorem 7.2.6).*

This unique matrix is called the positive square root. To compute this is extremely computationally expensive, as it requires, naively, the use of an eigenvalue decomposition, such that,

$$A = VQV^T,$$

where $A \in \mathbb{R}^{n \times n}$ is a symmetric positive semidefinite matrix, Q is the diagonal eigenvalue matrix and V the orthonormal eigenvectors matrix. The unique symmetric positive square root is thus,

$$B = VQ^{\frac{1}{2}}V^T,$$

however, to compute the eigenvalue problem, computation is an $\mathcal{O}(\frac{8}{3}n^3) + \mathcal{O}(n^2)$ algorithm (Pan and Chen, 1999).

However, we do not necessarily need the symmetry constraint to be enforced in this situation. Instead we look at the Cholesky decomposition which is instead $\mathcal{O}(\frac{1}{3}n^3) + \mathcal{O}(n^2)$ instead, which is much faster (ALGLIB, 1999).

To validate this as a valid optimization, we need to ensure that the constraints are all still satisfied by this change. As such, we need to find parameterizations of $A, B, \{C_j\}_{j=1:n}$ that maintain their respective constraints.

Lemma 20 *We can define A to be less computationally expensive by reformulating A as,*

$$A = \mathcal{L}W_AR_A^{-1},$$

where R_A is the upper Cholesky decomposition of $R_A^T R_A = \alpha_A \mathbf{I} + W_A^T W_A$, where R_A is the upper triangular matrix.

Proof We start by finding the Cholesky decomposition of $(\mathbf{I} + W_A^T W_A)^{-\frac{1}{2}}$, which must exist since the matrix is symmetric and positive definite, which implies that a Cholesky decomposition exists. It then follows that,

$$\alpha_A \mathbf{I} + W_A^T W_A = R_A^T R_A,$$

$$(\alpha_A \mathbf{I} + W_A^\top W_A)^{-1} = (R_A^\top R_A)^{-1} = R_A^{-1} R_A^{-\top}.$$

Note that R_A^{-1} is a Cholesky factor of the inverse, not the symmetric inverse square root (i.e. $R_A^{-1} \neq (\mathbf{I} + W_A^\top W_A)^{-\frac{1}{2}}$). We need to verify that this formulation satisfies the spectral norm constraint imposed on the system,

$$\begin{aligned} \mathcal{L}^2 &\geq \|A\|_2^2 = \lambda_{\max}(A^\top A) = \lambda_{\max}(AA^\top), \\ &= \mathcal{L}^2 \lambda_{\max}(W_A R_A^{-1} R_A^{-\top} W_A^\top), \\ &= \mathcal{L}^2 \lambda_{\max}(W_A (\alpha_A \mathbf{I} + W_A^\top W_A)^{-1} W_A^\top), \end{aligned}$$

which means that the spectral norm condition is still satisfied. ■

Similarly, we have that,

Lemma 21 *We can define $\{C_j\}_{j=1:n}$ to be less computationally expensive by reformulating $\{C_j\}_{j=1:n}$ as,*

$$C_j = \sqrt{2} W_j R_j^{-1} \begin{cases} \mathcal{L} \sqrt{\alpha_A} R_A^{-\top}, & j = 1 \\ \sqrt{2\alpha_{j-1}} R_{j-1}^{-\top}, & \text{else} \end{cases},$$

where R_j is the upper triangular Cholesky decomposition of $R_j^\top R_j = \Omega_j$.

Proof As a note, we need to satisfy the condition that,

$$2\mathbf{I} \succeq C_j \mathbf{D}_j^{-1} C_j^\top,$$

from Equations (7) and (8), where we thus decompose using Cholesky decomposition,

$$D_j = \begin{cases} \mathcal{L}^2 \alpha_A (\mathbf{I} + W_A^\top W_A)^{-1} = \mathcal{L}^2 \alpha_A R_A^{-1} R_A^{-\top}, & j = 1 \\ 2\alpha_{j-1} (\mathbf{I} + W_{j-1}^\top W_{j-1})^{-1} = 2\alpha_{j-1} R_{j-1}^{-1} R_{j-1}^{-\top}, & \text{else} \end{cases}.$$

For the case when $j = 1$, we have that,

$$\begin{aligned} C_1 \mathbf{D}_1^{-1} C_1^\top &= 2\mathcal{L}^2 \alpha_A W_1 R_1^{-1} R_A^{-\top} \left(\mathcal{L}^2 \alpha_A R_A^{-1} R_A^{-\top} \right)^{-1} R_A^{-1} R_1^{-\top} W_1^\top, \\ &= 2W_1 R_1^{-1} (R_A^{-\top} R_A^\top) (R_A R_A^{-1}) R_1^{-\top} W_1^\top, \\ &= 2W_1 (R_1^\top R_1)^{-1} W_1^\top, \\ &= 2W_1 (\alpha_1 \mathbf{I} + W_1 W_1^\top)^{-1} W_1^\top \preceq 2\mathbf{I}. \end{aligned}$$

Equivalently for the case when $j > 1$, we have that,

$$\begin{aligned} C_j \mathbf{D}_j^{-1} C_j^\top &= 4\alpha_{j-1} W_j R_j^{-1} R_{j-1}^{-\top} \left(2\alpha_{j-1} R_{j-1}^{-1} R_{j-1}^{-\top} \right)^{-1} R_{j-1}^{-1} R_j^{-\top} W_j^\top, \\ &= 2W_j R_j^{-1} (R_{j-1}^{-\top} R_{j-1}^\top) (R_{j-1} R_{j-1}^{-1}) R_j^{-\top} W_j^\top, \end{aligned}$$

following the same steps as for case $j = 1$, we have the same result. ■

Finally, we have the simplification for B as follows,

Lemma 22 *We can define B to be less computationally expensive by reformulating B as,*

$$B = cR_{\Sigma}^{-1}W_BR_B^{-1},$$

where R_{Σ} and R_B are the upper Cholesky decompositions of $\mathbf{I} + A\Sigma A^T$ and $\alpha_B\mathbf{I} + W_B^TW_B$ respectively, where R is an upper triangular matrix and $c = \sqrt{\|2\alpha_n(\alpha_n\mathbf{I} + W_nW_n^T)^{-1}\|_2}$.

Proof From Equation (10) we need to satisfy the condition that,

$$B^T (\mathbf{I} + A\Sigma A^T) B \preceq 2\mathbf{I} - C_n\mathbf{D}_n^{-1}C_n^T,$$

where we thus decompose using Cholesky decomposition,

$$\begin{aligned} 2\mathbf{I} - C_n\mathbf{D}_n^{-1}C_n^T &\succeq B^T (\mathbf{I} + A\Sigma A^T) B, \\ &\succeq c^2(R_B^{-T}W_B^TR_{\Sigma}^{-T})(R_{\Sigma}^TR_{\Sigma})(R_{\Sigma}^{-1}W_BR_B^{-1}), \\ &\succeq c^2R_B^{-T}W_B^T(R_{\Sigma}^{-T}R_{\Sigma}^T)(R_{\Sigma}R_{\Sigma}^{-1})W_BR_B^{-1}, \\ &\succeq c^2R_B^{-T}W_B^TW_BR_B^{-1}. \end{aligned}$$

By construction we know that $c^2\mathbf{I} \succeq 2\mathbf{I} - C_n\mathbf{D}_n^{-1}C_n^T$ as such,

$$\begin{aligned} R_B^{-T}W_B^TW_BR_B^{-1} &\preceq \mathbf{I}, \\ W_B^TW_B &\preceq R_B^TR_B, \\ W_B^TW_B &\preceq \alpha_B\mathbf{I} + W_B^TW_B. \end{aligned}$$

■

as well,

Lemma 23 *We can define B to be less computationally expensive by reformulating B as,*

$$B = \sqrt{2\alpha_n}R_{\Sigma}^{-1}W_BR_B^{-1}R_C^{-T},$$

where R_{Σ} , R_B and R_C are the upper Cholesky decompositions of $\mathbf{I} + A\Sigma A^T$, $\alpha_B\mathbf{I} + W_B^TW_B$ and Ω_n respectively, where R is an upper triangular matrix.

Proof From Equation (10) we need to satisfy the condition that,

$$B^T (\mathbf{I} + A\Sigma A^T) B \preceq 2\mathbf{I} - C_n\mathbf{D}_n^{-1}C_n^T,$$

where we thus decompose using Cholesky decomposition,

$$\begin{aligned} &= B^T (\mathbf{I} + A\Sigma A^T) B, \\ &= 2\alpha_n(R_C^{-1}R_B^{-T}W_B^TR_{\Sigma}^{-T})(R_{\Sigma}^TR_{\Sigma})(R_{\Sigma}^{-1}W_BR_B^{-1}R_C^{-T}), \\ &= 2\alpha_nR_C^{-1}R_B^{-T}W_B^T(R_{\Sigma}^{-T}R_{\Sigma}^T)(R_{\Sigma}R_{\Sigma}^{-1})W_BR_B^{-1}R_C^{-T}, \\ &= 2\alpha_nR_C^{-1}R_B^{-T}W_B^TW_BR_B^{-1}R_C^{-T} \end{aligned}$$

$$\preceq 2\alpha_n R_C^{-1} \mathbf{I} R_C^{-\top} = 2\alpha_n \Omega_n^{-1} = 2\alpha_n \left(\alpha_n \mathbf{I} + W_n W_n^\top \right)^{-1}$$

■

Theorem 24 *The inverse of an upper triangular matrix, if it exists, is upper triangular (Taboga, 2021).*

Theorem 25 *The product of two upper triangular matrices is upper triangular (Taboga, 2021).*

Considering that all operations employ triangular-triangular or triangular-dense matrix multiplication, it is evident that optimized multiplication routines capable of multiplying triangular matrices using more efficient computational methods, owing to their sparsity, can be implemented. However, PyTorch does not inherently possess this functionality, necessitating the creation of a custom CUDA kernel to implement this optimization. Although this minor optimization is insignificant compared to the substantial performance gains achieved by replacing the eigen-decomposition with the Cholesky decomposition function.

Lemma 26 *Let $B \in \mathbb{R}^{n \times n}$ be symmetric positive definite. Let $R \in \mathbb{R}^{n \times n}$ be the (unique) Cholesky factor with positive diagonal such that $R^\top R = B$, and let $S = B^{\frac{1}{2}}$ be the (unique) symmetric positive definite square root of B , for any $m, n \in \mathbb{N}$,*

$$\mathcal{H}_R := \{WR^{-1} : W \in \mathbb{R}^{m \times n}\}, \mathcal{H}_S := \{WS^{-1} : W \in \mathbb{R}^{m \times n}\},$$

coincide $\mathcal{H}_R = \mathcal{H}_S$, as such $W \rightarrow WR^{-1}$ and $W \rightarrow WS^{-1}$ have the same expressiveness.

Proof From Lemma 17, we know that there exists an orthonormal matrix Q such that $S^{-1} = R^{-1}Q$ and equivalently $R^{-1} = S^{-1}Q^\top$.

Let $A \in \mathcal{H}_S$. Then $A = WS^{-1}$ for some $W \in \mathbb{R}^{m \times n}$, we can thus

$$A = W(R^{-1}Q) = (WQ)R^{-1},$$

Since right-multiplication by the fixed invertible matrix Q is a bijection on $\mathbb{R}^{m \times n}$, the product WQ ranges over all $m \times n$ matrices as W , hence $A \in \mathcal{H}_R$.

Similarly let $A \in \mathcal{H}_R$. Then $A = WR^{-1}$ for some $W \in \mathbb{R}^{m \times n}$, we can thus

$$A = W(S^{-1}Q^\top) = (WQ^\top)S^{-1}.$$

As before, right-multiplication by Q^\top is a bijection on $\mathbb{R}^{m \times n}$, hence $A \in \mathcal{H}_S$.

Thus, the two parameterizations have identical representational power; they differ only by an orthogonal factor in the learnable parameter W . ■

From Lemma 26, we know that these less computationally expensive parameterizations of the parameters maintain the same level of expressiveness as their original parameterization.

Corollary 27 *The set of networks realizable by the Cholesky-based parameterization of $A, B, \{C_j\}_{j=1:n}$ is identical to that realizable by the symmetric square roots. Thus substituting the Cholesky factors for the symmetric ones, introduces no expressiveness loss, while greatly reducing the computation cost from $\mathcal{O}(\frac{8}{3}n^3)$ to $\mathcal{O}(\frac{1}{3}n)$.*

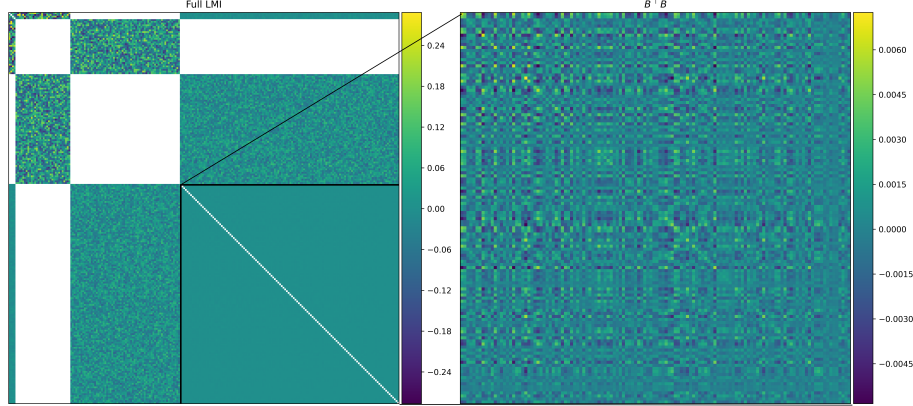


Figure 2: B matrix artifacting in network architecture with input and output size of 4 with layer widths of $[32, 64, 128]$ respectively

4.2 Convolution Layers

Let us define $h, w, k \in \mathbb{N}$, and $n = wh$. We define the input $x \in \mathbb{R}^{h \times w \times c_I}$, where $c_I, c_O \in \mathbb{N}$, represents the number of input and output channels for the image. We thus have the kernel $K \in \mathbb{R}^{c_O \times c_I \times k \times k}$ for which we assume that a circular convolution on $h \times w$ will be applied (Gray, 2005; Rao and Yip, 2018). Assuming circular boundary conditions, the parameterizations of $A, B, \{C_j\}_{j=1:n}$ can be interpreted in terms of the spectral frequency matrices, and in turn, the same normalization operations as above can be applied to them.

5 Other Architectures

5.1 Linear Network

It is possible to easily derive the same conditions as before for a classical deep neural network of the form,

$$\begin{aligned}
 x_{k+1} &= w_{k,n}, \\
 v_{k,1} &= C_1 x_k + b_1, \\
 w_{k,1} &= \sigma_1(v_{k,1}), \\
 &\vdots \\
 v_{k,n} &= C_n w_{k,n-1} + b_n, \\
 w_{k,n} &= \sigma_n(v_{k,n}).
 \end{aligned}$$

By simply setting $A_k = \mathbf{0}, B_k = \mathbf{I}$ from our residual structure. In turn, this results in the LMI, which generates the following conditions,

Lemma 28 *The result of D_1 is equal to the symmetric matrix,*

$$D_1 = \mathcal{L}^2 \mathbf{I} + 2L_1 m_1 C_1^\top \Lambda_1 C_1,$$

The result of \mathbf{D}_j for $j \in \{2, \dots, n\}$ is equal to the symmetric matrix,

$$\mathbf{D}_j = 2L_j m_j C_j^\top \Lambda_j C_j + 2\Lambda_j - (L_{j-1} + m_{j-1})^2 \Lambda_{j-1} C_{j-1} \mathbf{D}_{j-1}^{-1} C_{j-1}^\top \Lambda_{j-1},$$

The block triangular terms of \mathbf{L}_{ij} for $j = \{1, \dots, n\}$, where $\mathbf{L}_{jj} = \mathbf{I}$, are the following,

$$\begin{aligned} \mathbf{L}_{(j+1)j} &= -(L_j + m_j) \Lambda_j C_j \mathbf{D}_j^{-1}, \\ \mathbf{L}_{(j+2)j} &= \mathbf{0}, \\ &\vdots \\ \mathbf{L}_{(n+1)j} &= \mathbf{0}, \end{aligned}$$

where we define \mathbf{J}_j as the following: The symmetric block diagonal \mathbf{D}_n is of the form,

$$\mathbf{D}_{n+1} = 2\Lambda_n - \mathbf{I} - (L_n + m_n)^2 \Lambda_n C_n \mathbf{D}_n^{-1} C_n^\top \Lambda_n,$$

Again assuming $L_i = 1, m_j = 0$ and $\Lambda_j = \mathbf{I}$ for all j (same as in Section 3.2), for the sake of simplicity. In turn, we get the following simplified conditions,

$$\begin{aligned} \mathbf{D}_1 &= \mathcal{L}^2 \mathbf{I}, \\ \mathbf{D}_j &= 2\mathbf{I} - C_{j-1} \mathbf{D}_{j-1}^{-1} C_{j-1}^\top, \quad \forall j \in \{2, \dots, n\}, \\ \mathbf{D}_{n+1} &= \mathbf{I} - C_n \mathbf{D}_n^{-1} C_n^\top, \end{aligned}$$

where \mathbf{D}_1 is clearly always satisfied. In turn, the simplified constraints are defined as,

$$\begin{aligned} \kappa_j &= \begin{cases} 1, & j = n, \\ 2, & \text{else} \end{cases}, \\ C_j \mathbf{D}_j^{-1} C_j^\top &\prec \kappa_j \mathbf{I}, \quad \forall j \end{aligned}$$

which generates parameterization similar to the ones in Section 3.3,

Lemma 29 *For the linear network defined by the \mathcal{L} -Lipschitz activation function σ , the deep network's weights $\{C_j\}_{j=1:n}$ can be parameterized as,*

$$\begin{aligned} C_j &= \sqrt{\kappa_j} W_j (\alpha_j \mathbf{I} + W_j^\top W_j)^{-\frac{1}{2}} D_j^{\frac{1}{2}}, \quad \forall j \\ C_j &= \sqrt{\kappa_j \kappa_{j-1}} W_j R_j^{-1} R_{j-1}^{-\top}, \end{aligned}$$

where $R_j^\top R_j = \bar{\Omega}_j$.

$$\bar{\Omega}_j = \begin{cases} \mathbf{I}, & \text{if } j = 1 \\ \alpha_j \mathbf{I} + W_j W_j^\top, & \text{else} \end{cases}.$$

which also implies that, from the logic following from Lemma 16,

$$\mathbf{D}_j = \kappa_{j-1} (\mathbf{I} + W_{j-1} W_{j-1}^\top)^{-1}, \quad \forall j \in \{2, \dots, n\}.$$

this more expressive nature to current methodologies such as in Araujo et al. (2023); Prach and Lampert (2022); Meunier et al. (2021b); Singla et al. (2021) allow for an end-to-end \mathcal{L} -parameterization of the linear network, thus helping for mitigating decay initialization problems illustrated in Juston et al. (2025), where the approximated 1-Lipschitz deep neural network parameterizations of just stacking 1-Lipschitz layers and ensuring the 1-Lipschitz property causes decay due to these stacking approximations. This recursively dependent network, with the addition of the Cholesky decomposition parameterization in Section 4.1, provides an extremely computationally efficient and robust framework for deep Lipschitz networks.

5.2 U-Net

U-Nets (Ronneberger et al., 2015), a variant of variational latent state encoders (VAE), are effective at encoding information into a lower-dimensional latent space. These networks have been widely used in diffusion networks, data compression, and similar tasks (Rombach et al., 2021; Kingma and Welling, 2019). The network structure is as follows, assuming an U-Net of depth d , meaning that there are $n = 2d - 1$ blocks, starting with the encoder structure,

$$\begin{aligned} v_{k,1} &= C_1 x_k + b_1, \\ w_{k,1} &= \sigma_1(v_{k,1}), \\ &\vdots \\ v_{k,d} &= C_d w_{k,d-1} + b_d, \\ w_{k,d} &= \sigma_d(v_{k,d}). \end{aligned}$$

where $w_{k,d}$ represents the latent space encoding vector output. The decoder output is,

$$\begin{aligned} v_{k,d+1} &= C_{d+1,1} w_{k,d-1} + C_{d+1,2} w_{k,d} + b_{d+1}, \\ w_{k,d+1} &= \sigma_1(v_{k,d+1}), \\ &\vdots \\ v_{k,n} &= C_{n,1} w_{k,1} + C_{n,2} w_{k,n-1} + b_n, \\ w_{k,n} &= \sigma_n(v_{k,n}), \\ x_{k+1} &= w_{k,n} \end{aligned}$$

from which the full LMI and the set of constraints can be derived; these will be explored in a separate paper. Having a Lipschitz U-Net could provide interesting properties to the latent space representation encoding vector. Given that having a latent space with a Lipschitz bound enforces the distance between embeddings to be a Lipschitz bound as well. This formulation will be explored in future work.

6 Experiments

This Section goes through evaluating the LDL^\top network with other state-of-the-art algorithms on a series of data sets from the UCI machine learning repository and an analysis of the results.

6.1 UCI Machine Learning Repository Dataset

To validate and compare the performance of the LDL^\top based algorithms, we evaluated this work and other state-of-the-art techniques on a collection of 121 classification data sets from the UCI Machine Learning repository. These repositories encompass a wide variety of problems from physics, geology, and biology (Fernández-Delgado et al., 2014). The data sets range in size from 10 to 63 million data points, with input features ranging from 1 to 3.2 million. Because there are such a large number of data sets and some of the data sets have a prohibitively large amount of data for training, we instead look at a subset of these data sets whose data set subsection selection was provided by the previous works for SeLU (Klambauer et al., 2017), which selects 121 data sets and prepares them with four-fold cross-validation.

6.2 Details on the Architecture and Hyper-parameters

To ensure fairness among the chosen algorithms, each network was provided with a set depth of four hidden layers. A simple heuristic determined the network’s width, w , where

$$\begin{aligned} w &= \min(\max(4N, 32), 512), \\ w &= (1 + 0.25\mathbb{1}_{M>10})b, \\ w &= 2^{\text{round}(\log_2(b))}, \end{aligned}$$

and we have to choose the closest power-of-2 width for these data set widths, Table 1 demonstrates the different 1-Lipchitz architectures used and the parameter specifications during training across all data sets. In addition, all networks were trained using the AdamW optimizer with a weight decay of $1e-4$ and an initial learning rate of $1e-3$; a training scheduler was also used that halved the learning rate when validation accuracy plateaued for eight or more epochs. Each network was trained for a maximum of 100 epochs, and early termination was set to terminate the run if no improvement in validation accuracy was observed for 30 epochs. The loss function used was cross-entropy, and class weights were calculated to normalize the data sets’ uneven class distributions, especially in the smaller data sets. Each network was four layers deep, as adding more layers did not change rankings and is therefore deemed acceptable.

For simpler, consistent computation of certification accuracy, each network architecture was fitted with a linear normalization head as its last layer.

We first compare the mean accuracy of each algorithm to validate purely on accuracy, and we also compare the provable accuracy of each network in Table 2. For each model on each data set, we report both clean accuracy and certified robust accuracy at ℓ_2 radii 36/255, 72/255, 108/255, and 255/255, obtained from the global Lipschitz bound. Given a 1-Lipschitz network and a radius ϵ , we are guaranteed that predictions cannot change within an ℓ_2 ball of radius ϵ ; we therefore label a test point as certifiably correct at radius ϵ if the prediction of the datapoint matches the true label (Araujo et al., 2023). We can see that, in terms of accuracy, the Sandwich layer network consistently performs best among the other algorithms; however, between the LDLT and the SLL, the closest equivalent to this paper, the LDLT-R algorithm, consistently performs better than the SLL-based layers. The AOL algorithm consistently performed the worst among the algorithms. The Tables 3-4d provide

Algorithm	Width	Depth	Parameters	Padding	Input dim	Output dim
AOL	32—512	4—4	282—694837	10—524	3—262	2—100
Orthogonal	32—512	4—4	285—694840	10—524	3—262	2—100
Sandwich	32—512	4—4	615—1520140	10—524	3—262	2—100
SLL	32—512	4—4	1558—1084073	10—524	3—262	2—100
LDLT-L	32—512	4—4	3366—929297	10—524	3—262	2—100
LDLT-R	32—512	4—4	3463—1063442	10—524	3—262	2—100

Table 1: Model dimension ranges (min—max across all data sets and folds). Input/Output dimensions follow data set label spaces.

a statistical comparison of the different algorithms at different certified accuracy noise levels. The average ranks compare relative performance across many data sets without assuming scales (Demšar, 2006). This helps guard against a few easy data sets with large dominating means (Demšar, 2006). The Wilcoxon-based significant loss helps answer how often A performs significantly better than B across data sets, and the mean-aggregate scores show the absolute accuracy margins between the algorithms, which rank-based methods often ignore (Demšar, 2006).

From the ranking statistics from Tables 3-4 we can see that the Sandwich layers clearly dominate all the tests; however, the LDLT-R is always above the SLL layer rankings; however, for the general accuracy metric the LDLT-L barely ties with the Sandwich layers but does not handle the noise as well.

Algorithm	N	Accuracy	Certified Accuracy			
			36/255	72/255	108/255	255/255
AOL	121	0.6295 ± 0.2278	0.3669 ± 0.2895	0.2660 ± 0.2953	0.2076 ± 0.2819	0.0999 ± 0.1875
Orthogonal	121	0.6969 ± 0.1938	0.5973 ± 0.2386	0.5073 ± 0.2617	0.4300 ± 0.2702	0.1970 ± 0.2288
Sandwich	121	0.7215 ± 0.1871	0.6375 ± 0.2305	0.5593 ± 0.2503	0.4836 ± 0.2659	0.2496 ± 0.2471
SLL	121	0.6978 ± 0.1998	0.5885 ± 0.2451	0.4975 ± 0.2649	0.4146 ± 0.2715	0.1918 ± 0.2222
LDLT-L	121	0.7223 ± 0.1868	0.5301 ± 0.2920	0.4293 ± 0.3049	0.3535 ± 0.3003	0.1652 ± 0.2281
LDLT-R	121	0.7022 ± 0.1944	0.6107 ± 0.2314	0.5292 ± 0.2525	0.4492 ± 0.2655	0.2172 ± 0.2312

Table 2: Sorted mean \pm std across N data sets for each algorithm.

The Tables 5-6 show a graphical comparison of the pair-wise results between each of the algorithms from the Wilcoxon pair-wise test. The full summary of the results is provided in Appendix B. We can again see that, for the non-perturbed mean accuracy metric (Table 5), the LDLT-L, LDLT-R and Sandwich layers performed similarly, with the same number of victories. However, when looking at the perturbed certification accuracies, the Sandwich layers perform better than every other technique, while the LDLT-R only loses to the Sandwich layers.

Algorithm	Avg rank ↓	sig wins	sig losses	net wins	win share	mean r
LDLT-L	2.434	4	0	4	0.800	0.577
Sandwich	2.566	4	0	4	0.800	0.517
LDLT-R	3.438	1	2	-1	0.200	0.629
SLL	3.624	1	2	-1	0.200	0.678
Orthogonal	3.831	1	2	-1	0.200	0.639
AOL	5.107	0	5	-5	0.000	0.000

Table 3: Overall comparison on Mean Accuracy: average rank (lower is better) with Iman—Davenport $F = 44.33$ (df=5,600), $p = 1.11e - 16$; Nemenyi CD= 0.685. Counts are significant wins/losses after Holm within-metric at $\alpha = 0.05$.

Algorithm	Avg rank ↓	sig wins	sig losses	net wins	win share	mean r
Sandwich	2.021	5	0	5	1.000	0.626
LDLT-R	2.715	4	1	3	0.800	0.514
Orthogonal	3.417	2	2	0	0.400	0.627
SLL	3.426	2	2	0	0.400	0.602
LDLT-L	3.785	1	4	-3	0.200	0.732
AOL	5.636	0	5	-5	0.000	0.000

(a) Overall comparison on Mean Certified Accuracy (36/255): average rank (lower is better) with Iman—Davenport $F = 89.22$ (df=5,600), $p = 1.11e - 16$; Nemenyi CD= 0.685.

Algorithm	Avg rank ↓	sig wins	sig losses	net wins	win share	mean r
Sandwich	1.868	5	0	5	1.000	0.675
LDLT-R	2.562	4	1	3	0.800	0.548
Orthogonal	3.347	2	2	0	0.400	0.674
SLL	3.360	2	2	0	0.400	0.660
LDLT-L	4.136	1	4	-3	0.200	0.801
AOL	5.727	0	5	-5	0.000	0.000

(c) Overall comparison on Mean Certified Accuracy (108/255): average rank (lower is better) with Iman—Davenport $F = 125.70$ (df=5,600), $p = 1.11e - 16$; Nemenyi CD= 0.685.

Algorithm	Avg rank ↓	sig wins	sig losses	net wins	win share	mean r
Sandwich	1.926	5	0	5	1.000	0.670
LDLT-R	2.628	4	1	3	0.800	0.557
Orthogonal	3.376	2	2	0	0.400	0.643
SLL	3.409	2	2	0	0.400	0.640
LDLT-L	4.058	1	4	-3	0.200	0.732
AOL	5.603	0	5	-5	0.000	0.000

(b) Overall comparison on Mean Certified Accuracy (72/255): average rank (lower is better) with Iman—Davenport $F = 101.00$ (df=5,600), $p = 1.11e - 16$; Nemenyi CD= 0.685.

Algorithm	Avg rank ↓	sig wins	sig losses	net wins	win share	mean r
Sandwich	1.909	5	0	5	1.000	0.671
LDLT-R	2.550	4	1	3	0.800	0.575
SLL	3.310	2	2	0	0.400	0.662
Orthogonal	3.471	2	2	0	0.400	0.607
LDLT-L	4.202	1	4	-3	0.200	0.796
AOL	5.558	0	5	-5	0.000	0.000

(d) Overall comparison on Mean Certified Accuracy (255/255): average rank (lower is better) with Iman—Davenport $F = 105.79$ (df=5,600), $p = 1.11e - 16$; Nemenyi CD= 0.685.

Table 4: Overall comparison on Mean Certified Accuracy at perturbation radii 36/255, 72/255, 108/255, and 255/255. Counts are significant wins/losses after Holm within-metric at $\alpha = 0.05$.

7 Limitations

ResNet is numerically unstable in deep networks unless more robust Cholesky-update routines are implemented. The convolution implementation of the network is computationally expensive due to the cost of complex operators and the doubling of matrix sizes in the block-

	AOL	LDLT-L	LDLT-R	Orthogonal	Sandwich	SLL
AOL	.	▼	▼	▼	▼	▼
LDLT-L	▲	.	▲	▲	.	▲
LDLT-R	▲	▼	.	.	▼	.
Orthogonal	▲	▼	.	.	▼	.
Sandwich	▲	.	▲	▲	.	▲
SLL	▲	▼	.	.	▼	.

Table 5: Pairwise Wilcoxon outcomes for Mean Accuracy (Holm within-metric at $\alpha = 0.05$): row vs. column (▲ win, ▼ loss, . none).

	AOL	LDLT-L	LDLT-R	Orthogonal	Sandwich	SLL
AOL	.	▼	▼	▼	▼	▼
LDLT-L	▲	.	▼	▼	▼	▼
LDLT-R	▲	▲	.	▲	▼	▲
Orthogonal	▲	▲	▼	.	▼	.
Sandwich	▲	▲	▲	▲	.	▲
SLL	▲	▲	▼	.	▼	.

(a) Pairwise Wilcoxon outcomes for Mean Certified Accuracy (36/255).

	AOL	LDLT-L	LDLT-R	Orthogonal	Sandwich	SLL
AOL	.	▼	▼	▼	▼	▼
LDLT-L	▲	.	▼	▼	▼	▼
LDLT-R	▲	▲	.	▲	▼	▲
Orthogonal	▲	▲	▼	.	▼	.
Sandwich	▲	▲	▲	▲	.	▲
SLL	▲	▲	▼	.	▼	.

(c) Pairwise Wilcoxon outcomes for Mean Certified Accuracy (108/255).

	AOL	LDLT-L	LDLT-R	Orthogonal	Sandwich	SLL
AOL	.	▼	▼	▼	▼	▼
LDLT-L	▲	.	▼	▼	▼	▼
LDLT-R	▲	▲	.	▲	▼	▲
Orthogonal	▲	▲	▼	.	▼	.
Sandwich	▲	▲	▲	▲	.	▲
SLL	▲	▲	▼	.	▼	.

(b) Pairwise Wilcoxon outcomes for Mean Certified Accuracy (72/255).

	AOL	LDLT-L	LDLT-R	Orthogonal	Sandwich	SLL
AOL	.	▼	▼	▼	▼	▼
LDLT-L	▲	.	▼	▼	▼	▼
LDLT-R	▲	▲	.	▲	▼	▲
Orthogonal	▲	▲	▼	.	▼	.
Sandwich	▲	▲	▲	▲	.	▲
SLL	▲	▲	▼	.	▼	.

(d) Pairwise Wilcoxon outcomes for Mean Certified Accuracy (255/255).

Table 6: Overall pairwise Wilcoxon outcomes on Mean Certified Accuracy at perturbation radii 36/255, 72/255, 108/255, and 255/255. row vs. column (▲ win, ▼ loss, . tie). Holm within-metric at $\alpha = 0.05$.

matrix representation. PyTorch is currently working on implementing less computationally expensive complex operations (cf. <https://github.com/openteams-ai/pytorch-complex-tensor>, for details). Training networks for complex data sets like CIFAR10, CIFAR100, or TinyImageNet becomes prohibitively expensive due to the scaling of CNN computational cost. These data sets require greater convolutional channel depths for effectiveness. Future work involves developing these additional data sets and validations.

8 Conclusion

We introduced a novel LDL^\top framework to decompose the LMI into block matrices D , the only components needing constraints. This enables complex architectures to derive and

enforce their constraints. The deep residual network structure and deep linear network are demonstrated through an end-to-end analysis, not a shallow layer-by-layer perspective.

This architecture offers greater robustness to adversarial noise than its direct competitor, the SDP-Layers (Araujo et al., 2023), and outperforms other state-of-the-art algorithms. The residual structure LDLT-R consistently ranks higher than the SLL layers, achieving 3%-13% better performance at higher certified accuracy thresholds. The Sandwich layers (Wang and Manchester, 2023) perform best among the selected algorithms. Based on the empirical accuracy increase from the Sandwich layers, we will explore integrating their parameterization into our system to achieve further accuracy. In the future, U-Nets, with their 1-Lipschitz latent-state representation, could be considered for specific applications or unknown beneficial properties. Novel normalization schemes based on the current network architecture will be derived to improve training efficiency. From the LDL^\top decomposition formulation, this methodology enables decomposing neural networks into linear and non-linear operations and generating both the LMI and its parametric LDL^\top decomposition for general architectures.

This methodology, derived from the LDL^\top decomposition formulation, enables the creation of an algorithmic method for decomposing neural networks into linear and non-linear operations, generating both the LMI and its parametric LDL^\top decomposition for general architectures.

9 Code

The code for this repository, including the models and their respective training weights, is located at <https://github.com/Marius-Juston/DeepLipschitzResNet>. With the trained weights and Tensorboard plots available for download at the HuggingFace repository location <https://huggingface.co/SuperComputer/LDLT>.

10 Declaration of Generative AI and AI-assisted technologies in the writing process

During the preparation of this work, the authors used ChatGPT (OpenAI) to improve the clarity and fluency of the English text. After using this tool, the author reviewed and edited the content as needed and takes full responsibility for the publication’s content.

Acknowledgments and Disclosure of Funding

This research was supported in part by the U.S. Army Corps of Engineers Engineering Research and Development Center, Construction Engineering Research Laboratory under Grant W9132T23C0013.

The authors declare that they have no known competing financial interests or personal relationships that could have appeared to influence the work reported in this paper.

Appendix A. Activation Function Quadratic Bounds

For the sake of completeness, the L and m constants of the activation functions defined in PyTorch (assuming default values if not specified) were derived and defined in Table 7. It should be noted that the Hardshrink and RReLU could not be used due to their infinite L, m constants; Hardshrink has infinite L, m due to its noncontinuous piece-wise definition, and PReLU due to its stochastic definition, which no longer made its L, m computable. To compute the bounds L, m bounds of the activation functions revolved to finding the minimum and maximum gradient of each activation function, $f(x)$.

$$m = \arg \min_x \frac{\partial f(x)}{\partial x}, \quad L = \arg \max_x \frac{\partial f(x)}{\partial x} \quad (18)$$

Where,

$$\operatorname{erfc}(z) = 1 - \operatorname{erf}(z), \quad \operatorname{erf}(z) = \frac{2}{\sqrt{\pi}} \int_0^z e^{-t^2} dt. \quad (19)$$

Activation Function	L	m	S	P
ELU ($\alpha = 1$) (Clevert et al., 2015)	$\max(1, \alpha)$	0	$\max(1, \alpha)$	0
Hardshrink (Cancino-De-Greiff et al., 2002)	∞	0	∞	∞
Hardsigmoid (Courbariaux et al., 2015)	$\frac{1}{6}$	0	$\frac{1}{6}$	0
Hardtanh (Collobert, 2004)	1	0	1	0
Hardswish (Howard et al., 2019)	1.5	-0.5	1	-0.75
LeakyReLU ($\alpha = 10^{-2}$) (Maas et al., 2013)	1	α	$1 + \alpha$	α
LogSigmoid	1	0	1	0
PReLU ($\alpha = \frac{1}{4}$) (He et al., 2015a)	1	α	$1 + \alpha$	α
ReLU (McCulloch and Pitts, 1943)	1	0	1	0
ReLU6 (Howard et al., 2017)	1	0	1	0
RReLU (Xu et al., 2015)	∞	$-\infty$	∞	∞
SELU (Klambauer et al., 2017)	$\alpha \cdot \text{scale}$ ≈ 1.758099341	0	$\alpha \cdot \text{scale}$ ≈ 1.758099341	0
CELU (Barron, 2017)	1	0	1	0
	$\frac{\operatorname{erfc}(1)}{2} - \frac{1}{e\sqrt{\pi}}$	$\frac{1}{2}(\operatorname{erf}(1) + 1) + \frac{1}{e\sqrt{\pi}}$		$\frac{(e\sqrt{\pi}(\operatorname{erf}(1) + 1) + 2)(e\sqrt{\pi}\operatorname{erfc}(1) - 2)}{4e^2\pi}$
GELU (Hendrycks and Gimpel, 2016)	≈ 1.128904145	≈ -0.1289041452	1	≈ -0.145520424
Sigmoid (Sak et al., 2014)	1	0	1	0
SiLU (Elfwing et al., 2017)	1.099839320	-0.09983932013	1	-0.1098072100
Softplus (Zhou, 2016)	1	0	1	0
Mish ($\alpha \geq \frac{1}{2}$) (Misra, 2019)	1.199678640	-0.2157287822	0.8060623125	-0.2204297485
Softshrink (Cancino-De-Greiff et al., 2002)	1	0	1	0
Softsign (Ping et al., 2017)	1	0	1	0
Tanh (Sak et al., 2014)	1	0	1	0
Tanhshrink	1	0	1	0
Threshold	1	0	1	0

Table 7: Convexity constants of the element-wise activation functions in PyTorch.

Appendix B. Wilcoxon Metrics

The general metrics for all runs, with more details on pairwise Wilcoxon comparisons for all 121 UCI data sets between each algorithm can be found in Tables 8-12, which shows the complete decompositions of win and loss ratios between the different algorithms over all 121 UCI data sets.

Algorithms		Run Statistics						Wilcoxon pairwise Statistics					
Alg A	Alg B	n	wins _A	wins _B	ties	WinRate A	Median Δ (A—B)	W	p	$p_{\text{Holm,within}}$	$p_{\text{Holm,global}}$	r	
AOL	LDLT-L	121	16	105	0	0.1322	-0.0568	412	$2.3e-17^{***}$	$3.4e-16^{***}$	0 ^{***}	0.7708	
AOL	Sandwich	121	18	103	0	0.1488	-0.0595	518	$2.3e-16^{***}$	0 ^{***}	0 ^{***}	0.7459	
AOL	SLL	121	22	99	0	0.1818	-0.0351	806	0 ^{***}	0 ^{***}	0 ^{***}	0.6782	
AOL	Orthogonal	121	27	94	0	0.2231	-0.0265	971	0 ^{***}	0 ^{***}	$1.0e-10^{***}$	0.6394	
AOL	LDLT-R	121	25	96	0	0.2066	-0.0313	1013	0 ^{***}	0 ^{***}	$2.0e-10^{***}$	0.6295	
Orthogonal	Sandwich	121	31	89	1	0.2603	-0.0126	1269	$6.0e-10^{***}$	$6.3e-09^{***}$	$2.2e-08^{***}$	0.5643	
LDLT-L	Orthogonal	121	94	27	0	0.7769	0.0139	1309	$7.0e-10^{***}$	$6.6e-09^{***}$	$2.5e-08^{***}$	0.5599	
LDLT-L	SLL	121	86	35	0	0.7107	0.0111	1503	$1.5e-08^{***}$	$1.2e-07^{***}$	$4.9e-07^{***}$	0.5143	
LDLT-L	LDLT-R	121	87	33	1	0.7231	0.0108	1689	$3.7e-07^{***}$	$2.6e-06^{***}$	$1.1e-05^{***}$	0.4639	
Sandwich	SLL	121	83	38	0	0.6860	0.0090	1789	$8.8e-07^{***}$	$5.3e-06^{***}$	$2.3e-05^{***}$	0.4470	
LDLT-R	Sandwich	121	43	78	0	0.3554	-0.0068	2364	$6.0e-04^{***}$	$3.0e-03^{**}$	$7.2e-03^{**}$	0.3118	
LDLT-R	SLL	121	66	54	1	0.5496	0.0019	3070	$1.4e-01$	$5.7e-01$	$8.7e-01$	0.1338	
LDLT-R	Orthogonal	121	71	50	0	0.5868	0.0025	3138	$1.5e-01$	$5.7e-01$	$8.7e-01$	0.1298	
Orthogonal	SLL	121	60	61	0	0.4959	-0.0004	3623	$8.6e-01$	$1.0e+00$	$1.0e+00$	0.0158	
LDLT-L	Sandwich	121	59	62	0	0.4876	-0.0002	3624	$8.6e-01$	$1.0e+00$	$1.0e+00$	0.0155	

Stars mark significance (* $p \leq 0.05$, ** $p \leq 0.01$, *** $p \leq 0.001$).

Table 8: Wilcoxon signed-rank tests (two-sided) for Mean Accuracy; p -values with Holm FWER corrections within-metric and global.

Algorithms		Run Statistics						Wilcoxon pairwise Statistics					
Alg A	Alg B	n	wins _A	wins _B	ties	WinRate A	Median	W	p	$p_{\text{Holm,within}}$	$p_{\text{Holm,global}}$	r	
							Δ (A—B)						
AOL	LDLT-R	121	6	115	0	0.0496	-0.2319	84	$1.1e-20^{***}$	$1.6e-19^{***}$	$7.7e-19^{***}$	0.8479	
AOL	Sandwich	121	6	115	0	0.0496	-0.2436	88	$1.2e-20^{***}$	$1.7e-19^{***}$	$8.4e-19^{***}$	0.8470	
AOL	SLL	121	6	115	0	0.0496	-0.1912	145	$4.8e-20^{***}$	$6.2e-19^{***}$	$3.2e-18^{***}$	0.8336	
AOL	Orthogonal	121	10	111	0	0.0826	-0.2187	196	$1.6e-19^{***}$	$1.9e-18^{***}$	$1.0e-17^{***}$	0.8216	
AOL	LDLT-L	121	16	105	0	0.1322	-0.1218	579	$8.5e-16^{***}$	0***	0***	0.7315	
LDLT-L	Sandwich	121	28	93	0	0.2314	-0.0511	884	0***	0***	0***	0.6598	
Orthogonal	Sandwich	121	24	96	1	0.2025	-0.0275	1002	0***	0***	$2.0e-10^{***}$	0.6282	
Sandwich	SLL	121	97	24	0	0.8017	0.0199	1005	0***	0***	$2.0e-10^{***}$	0.6314	
LDLT-L	LDLT-R	121	39	82	0	0.3223	-0.0372	1356	$1.6e-09^{***}$	$1.1e-08^{***}$	$5.2e-08^{***}$	0.5488	
LDLT-L	Orthogonal	121	47	74	0	0.3884	-0.0190	1855	$2.1e-06^{***}$	$1.2e-05^{***}$	$4.8e-05^{***}$	0.4315	
LDLT-R	SLL	121	81	39	1	0.6736	0.0118	2104	$6.5e-05^{***}$	$2.5e-04^{***}$	$1.0e-03^{***}$	0.3647	
LDLT-L	SLL	121	49	72	0	0.4050	-0.0075	2119	$4.8e-05^{***}$	$2.4e-04^{***}$	$9.2e-04^{***}$	0.3694	
LDLT-R	Sandwich	121	41	80	0	0.3388	-0.0168	2142	$6.2e-05^{***}$	$2.5e-04^{***}$	$1.0e-03^{***}$	0.3640	
LDLT-R	Orthogonal	121	78	43	0	0.6446	0.0126	2429	$1.1e-03^{**}$	$2.2e-03^{**}$	$1.1e-02^*$	0.2965	
Orthogonal	SLL	121	60	61	0	0.4959	-0.0004	3076	$1.1e-01$	$1.1e-01$	$8.7e-01$	0.1444	

Stars mark significance (* $p \leq 0.05$, ** $p \leq 0.01$, *** $p \leq 0.001$).

Table 9: Wilcoxon signed-rank tests (two-sided) for Mean Certified Accuracy (36/255); p -values with Holm FWER corrections within-metric and global.

References

Etika Agarwal, S. Sivaranjani, Vijay Gupta, and Panos Antsaklis. Sequential synthesis of distributed controllers for cascade interconnected systems. *Proceedings of the American Control Conference*, 2019-July:5816–5821, 7 2019. ISSN 07431619. doi: 10.23919/ACC.2019.8814701.

LDLT \mathcal{L} -LIPSCHITZ NETWORK

Algorithms		Run Statistics						Wilcoxon pairwise Statistics					
Alg A	Alg B	n	wins _A	wins _B	ties	WinRate A	Median	W	p	$p_{\text{Holm,within}}$	$p_{\text{Holm,global}}$	r	
							Δ (A—B)						
AOL	Sandwich	121	7	114	0	0.0579	-0.2614	107	$1.9e-20^{***}$	$2.9e-19^{***}$	$1.3e-18^{***}$	0.8425	
AOL	LDLT-R	121	5	116	0	0.0413	-0.2327	116	$2.4e-20^{***}$	$3.3e-19^{***}$	$1.6e-18^{***}$	0.8404	
AOL	SLL	121	5	116	0	0.0413	-0.1928	162	$7.1e-20^{***}$	$9.3e-19^{***}$	$4.6e-18^{***}$	0.8296	
AOL	Orthogonal	121	11	110	0	0.0909	-0.2064	214	$2.4e-19^{***}$	$2.9e-18^{***}$	$1.5e-17^{***}$	0.8174	
AOL	LDLT-L	121	19	100	2	0.1653	-0.1250	557	0 ^{***}	0 ^{***}	0 ^{***}	0.7323	
Orthogonal	Sandwich	121	19	101	1	0.1612	-0.0346	601	0 ^{***}	0 ^{***}	0 ^{***}	0.7240	
LDLT-L	Sandwich	121	20	101	0	0.1653	-0.0772	607	0 ^{***}	0 ^{***}	0 ^{***}	0.7250	
Sandwich	SLL	121	95	25	1	0.7893	0.0393	801	0 ^{***}	0 ^{***}	0 ^{***}	0.6762	
LDLT-L	LDLT-R	121	30	91	0	0.2479	-0.0627	930	0 ^{***}	0 ^{***}	0 ^{***}	0.6490	
LDLT-L	Orthogonal	121	42	79	0	0.3471	-0.0210	1696	$2.5e-07^{***}$	$1.5e-06^{***}$	$7.5e-06^{***}$	0.4689	
LDLT-L	SLL	121	42	79	0	0.3471	-0.0213	1776	$7.4e-07^{***}$	$3.7e-06^{***}$	$2.0e-05^{***}$	0.4501	
LDLT-R	SLL	121	83	38	0	0.6860	0.0192	1938	$5.9e-06^{***}$	$2.3e-05^{***}$	$1.3e-04^{***}$	0.4120	
LDLT-R	Sandwich	121	40	81	0	0.3306	-0.0197	2062	$2.5e-05^{***}$	$7.6e-05^{***}$	$5.2e-04^{***}$	0.3828	
LDLT-R	Orthogonal	121	78	43	0	0.6446	0.0178	2306	$3.4e-04^{***}$	$6.9e-04^{***}$	$4.5e-03^{**}$	0.3254	
Orthogonal	SLL	121	66	55	0	0.5455	0.0041	3178	$1.9e-01$	$1.9e-01$	$8.7e-01$	0.1204	

Stars mark significance (* $p \leq 0.05$, ** $p \leq 0.01$, *** $p \leq 0.001$).

Table 10: Wilcoxon signed-rank tests (two-sided) for Mean Certified Accuracy (72/255); p -values with Holm FWER corrections within-metric and global.

Algorithms		Run Statistics						Wilcoxon pairwise Statistics					
Alg A	Alg B	n	wins _A	wins _B	ties	WinRate A	Median Δ (A—B)	W	p	$p_{\text{Holm,within}}$	$p_{\text{Holm,global}}$	r	
AOL	LDLT-R	121	1	120	0	0.0083	-0.2229	11	$1.8e-21^{***}$	$2.7e-20^{***}$	$1.3e-19^{***}$	0.8651	
AOL	SLL	121	4	117	0	0.0331	-0.1616	33	$3.1e-21^{***}$	$4.3e-20^{***}$	$2.3e-19^{***}$	0.8599	
AOL	Orthogonal	121	6	115	0	0.0496	-0.1829	54	$5.2e-21^{***}$	$6.8e-20^{***}$	$3.8e-19^{***}$	0.8550	
AOL	Sandwich	121	5	116	0	0.0413	-0.2530	63	$6.5e-21^{***}$	$7.8e-20^{***}$	$4.7e-19^{***}$	0.8529	
AOL	LDLT-L	121	15	102	4	0.1405	-0.0795	265	$4.5e-18^{***}$	$5.0e-17^{***}$	$2.7e-16^{***}$	0.8011	
LDLT-L	Sandwich	121	16	104	1	0.1364	-0.0911	469	$1.3e-16^{***}$	0***	0***	0.7556	
Orthogonal	Sandwich	121	15	106	0	0.1240	-0.0411	634	0***	0***	0***	0.7186	
Sandwich	SLL	121	95	25	1	0.7893	0.0391	769	0***	0***	0***	0.6839	
LDLT-L	LDLT-R	121	28	93	0	0.2314	-0.0559	854	0***	0***	0***	0.6669	
LDLT-L	Orthogonal	121	39	82	0	0.3223	-0.0289	1595	$6.0e-08^{***}$	$3.6e-07^{***}$	$1.9e-06^{***}$	0.4926	
LDLT-L	SLL	121	37	82	2	0.3140	-0.0231	1675	$5.1e-07^{***}$	$2.5e-06^{***}$	$1.4e-05^{***}$	0.4605	
LDLT-R	SLL	121	83	38	0	0.6860	0.0187	2059	$2.5e-05^{***}$	$9.8e-05^{***}$	$5.2e-04^{***}$	0.3835	
LDLT-R	Sandwich	121	43	78	0	0.3554	-0.0213	2138	$6.0e-05^{***}$	$1.8e-04^{***}$	$1.0e-03^{**}$	0.3649	
LDLT-R	Orthogonal	121	77	44	0	0.6364	0.0182	2506	$2.2e-03^{**}$	$4.4e-03^{**}$	$2.0e-02^*$	0.2784	
Orthogonal	SLL	121	65	56	0	0.5372	0.0038	3069	$1.1e-01$	$1.1e-01$	$8.7e-01$	0.1460	

Stars mark significance (* $p \leq 0.05$, ** $p \leq 0.01$, *** $p \leq 0.001$).

Table 11: Wilcoxon signed-rank tests (two-sided) for Mean Certified Accuracy (108/255); p -values with Holm FWER corrections within-metric and global.

ALGLIB. Cholesky decomposition - C++, C#, Java library, 1999. URL <https://www.alglib.net/matrixops/cholesky.php>.

Alexandre Araujo, Aaron Havens, Blaise Delattre, Alexandre Allauzen, and Bin Hu. A unified algebraic perspective on lipschitz neural networks. 3 2023. URL <http://arxiv.org/abs/2303.03169>.

Algorithms		Run Statistics						Wilcoxon pairwise Statistics					
Alg A	Alg B	n	wins _A	wins _B	ties	WinRate A	Median	W	p	$p_{\text{Holm,within}}$	$p_{\text{Holm,global}}$	r	
							Δ (A—B)						
AOL	LDLT-R	121	1	111	9	0.0455	-0.0570	10	$5.4e-20^{***}$	$8.2e-19^{***}$	$3.6e-18^{***}$	0.8651	
AOL	SLL	121	3	104	14	0.0826	-0.0476	23	$5.3e-19^{***}$	$6.9e-18^{***}$	$3.2e-17^{***}$	0.8610	
AOL	Sandwich	121	2	112	7	0.0455	-0.0803	62	$9.9e-20^{***}$	$1.4e-18^{***}$	$6.3e-18^{***}$	0.8514	
AOL	Orthogonal	121	5	105	11	0.0868	-0.0363	122	$2.4e-18^{***}$	$2.8e-17^{***}$	$1.4e-16^{***}$	0.8331	
AOL	LDLT-L	121	8	85	28	0.1818	-0.0160	182	0^{***}	0^{***}	0^{***}	0.7958	
Orthogonal	Sandwich	121	11	103	7	0.1198	-0.0313	258	$1.4e-17^{***}$	$1.5e-16^{***}$	$8.1e-16^{***}$	0.7995	
LDLT-L	Sandwich	121	12	102	7	0.1281	-0.0397	342	$1.1e-16^{***}$	0^{***}	0^{***}	0.7772	
LDLT-L	LDLT-R	121	23	89	9	0.2273	-0.0242	927	$1.0e-10^{***}$	$6.0e-10^{***}$	$3.0e-09^{***}$	0.6135	
Sandwich	SLL	121	90	25	6	0.7686	0.0240	977	0^{***}	$4.0e-10^{***}$	$1.7e-09^{***}$	0.6135	
LDLT-L	SLL	121	27	79	15	0.2851	-0.0091	1323	$1.9e-06^{***}$	$9.4e-06^{***}$	$4.5e-05^{***}$	0.4629	
LDLT-R	SLL	121	80	35	6	0.6860	0.0175	1603	$1.4e-06^{***}$	$8.1e-06^{***}$	$3.4e-05^{***}$	0.4506	
LDLT-L	Orthogonal	121	36	75	10	0.3388	-0.0085	1741	$5.8e-05^{***}$	$2.3e-04^{***}$	$1.0e-03^{**}$	0.3816	
LDLT-R	Orthogonal	121	77	40	4	0.6529	0.0132	1982	$6.5e-05^{***}$	$2.3e-04^{***}$	$1.0e-03^{**}$	0.3694	
LDLT-R	Sandwich	121	45	73	3	0.3843	-0.0078	2234	$6.1e-04^{***}$	$1.2e-03^{**}$	$7.2e-03^{**}$	0.3154	
Orthogonal	SLL	121	55	58	8	0.4876	0.0000	3068	$6.6e-01$	$6.6e-01$	$1.0e+00$	0.0410	

Stars mark significance (* $p \leq 0.05$, ** $p \leq 0.01$, *** $p \leq 0.001$).

Table 12: Wilcoxon signed-rank tests (two-sided) for Mean Certified Accuracy (255/255); p -values with Holm FWER corrections within-metric and global.

Shayan Aziznejad, Harshit Gupta, Joaquim Campos, and Michael Unser. Deep neural networks with trainable activations and controlled lipschitz constant. *IEEE Transactions on Signal Processing*, 68:4688–4699, 1 2020. doi: 10.1109/TSP.2020.3014611. URL <http://arxiv.org/abs/2001.06263><http://dx.doi.org/10.1109/TSP.2020.3014611>.

Jonathan T. Barron. Continuously differentiable exponential linear units. 4 2017. URL <http://arxiv.org/abs/1704.07483>.

Peter L. Bartlett, Dylan J. Foster, and Matus Telgarsky. Spectrally-normalized margin bounds for neural networks. *Advances in Neural Information Processing Systems*, 2017-December:6241–6250, 6 2017. ISSN 10495258. URL <https://arxiv.org/abs/1706.08498v2>.

Jay Bear, Adam Prügel-Bennett, and Jonathon Hare. Rethinking deep thinking: Stable learning of algorithms using lipschitz constraints. 10 2024. URL <https://arxiv.org/abs/2410.23451v1>.

Hector F. Cancino-De-Greiff, Rubensy Ramos-Garcia, and Juan V. Lorenzo-Ginori. Signal de-noising in magnetic resonance spectroscopy using wavelet transforms. *Concepts in Magnetic Resonance*, 14:388–401, 1 2002. ISSN 1043-7347. doi: 10.1002/cmr.10043. URL <https://onlinelibrary.wiley.com/doi/10.1002/cmr.10043>.

Djork-Arné Clevert, Thomas Unterthiner, and Sepp Hochreiter. Fast and accurate deep network learning by exponential linear units (elus). *4th International Conference on Learning Representations, ICLR 2016 - Conference Track Proceedings*, 11 2015. URL <http://arxiv.org/abs/1511.07289>.

Ronan Collobert. *Large Scale Machine Learning*. PhD thesis, Université de Paris VI, 2004.

- Matthieu Courbariaux, Yoshua Bengio, and Jean Pierre David. Binaryconnect: Training deep neural networks with binary weights during propagations. *Advances in Neural Information Processing Systems*, 2015-January:3123–3131, 11 2015. ISSN 10495258. URL <https://arxiv.org/abs/1511.00363v3>.
- Janez Demšar. Statistical Comparisons of Classifiers over Multiple Data Sets. *Journal of Machine Learning Research*, 7(1):1–30, 2006. ISSN 1533-7928. URL <http://jmlr.org/papers/v7/demsar06a.html>.
- Stefan Elfving, Eiji Uchibe, and Kenji Doya. Sigmoid-weighted linear units for neural network function approximation in reinforcement learning. *Neural Networks*, 107:3–11, 2 2017. ISSN 18792782. doi: 10.1016/j.neunet.2017.12.012. URL <https://arxiv.org/abs/1702.03118v3>.
- Mahyar Fazlyab, Alexander Robey, Hamed Hassani, Manfred Morari, and George J. Pappas. *Efficient and accurate estimation of lipschitz constants for deep neural networks*. Curran Associates Inc., Red Hook, NY, USA, 2019a.
- Mahyar Fazlyab, Alexander Robey, Hamed Hassani, Manfred Morari, and George J Pappas. Efficient and accurate estimation of lipschitz constants for deep neural networks, 2019b.
- Manuel Fernández-Delgado, Eva Cernadas, Senén Barro, Dinani Amorim, and Amorim Fernández-Delgado. Do we Need Hundreds of Classifiers to Solve Real World Classification Problems? *Journal of Machine Learning Research*, 15(90):3133–3181, 2014. ISSN 1533-7928. URL <http://jmlr.org/papers/v15/delgado14a.html>.
- Ian J. Goodfellow, Jonathon Shlens, and Christian Szegedy. Explaining and harnessing adversarial examples. *3rd International Conference on Learning Representations, ICLR 2015 - Conference Track Proceedings*, 12 2014. URL <https://arxiv.org/abs/1412.6572v3>.
- Henry Gouk, Eibe Frank, Bernhard Pfahringer, and Michael J. Cree. Regularisation of neural networks by enforcing lipschitz continuity. *Machine Learning*, 110:393–416, 2 2021. ISSN 0885-6125. doi: 10.1007/s10994-020-05929-w. URL <http://link.springer.com/10.1007/s10994-020-05929-w>.
- Robert M. Gray. Toeplitz and Circulant Matrices: A Review. *Foundations and Trends® in Communications and Information Theory*, 2(3):155–239, 2005. ISSN 1567-2190. doi: 10.1561/01000000006. URL <http://www.nowpublishers.com/article/Details/CIT-006>.
- Aaron J Havens, Alexandre Araujo, Siddharth Garg, Farshad Khorrami, and Bin Hu. Exploiting Connections between Lipschitz Structures for Certifiably Robust Deep Equilibrium Models. *Advances in Neural Information Processing Systems*, 36:21658–21674, 12 2023. URL <https://github.com/AaronHavens/ExploitingLipschitzDEQ>.
- Kaiming He, Xiangyu Zhang, Shaoqing Ren, and Jian Sun. Delving deep into rectifiers: Surpassing human-level performance on imagenet classification. *CoRR*, abs/1502.01852, 2 2015a. URL <http://arxiv.org/abs/1502.01852>.

- Kaiming He, Xiangyu Zhang, Shaoqing Ren, and Jian Sun. Deep residual learning for image recognition. *Proceedings of the IEEE Computer Society Conference on Computer Vision and Pattern Recognition*, 2016-December:770–778, 12 2015b. ISSN 10636919. doi: 10.1109/CVPR.2016.90. URL <https://arxiv.org/abs/1512.03385v1>.
- Dan Hendrycks and Kevin Gimpel. Gaussian error linear units (gelus). 6 2016. URL <https://arxiv.org/abs/1606.08415v5>.
- Nicholas J. Higham. Newton’s Method for the Matrix Square Root. *Mathematics of Computation*, 46(174):537, 4 1986. ISSN 00255718. doi: 10.2307/2007992.
- Roger A. Horn and Charles R. Johnson. Matrix Analysis. *Matrix Analysis*, 10 2012. doi: 10.1017/CBO9781139020411.
- Andrew Howard, Mark Sandler, Bo Chen, Weijun Wang, Liang Chieh Chen, Mingxing Tan, Grace Chu, Vijay Vasudevan, Yukun Zhu, Ruoming Pang, Quoc Le, and Hartwig Adam. Searching for mobilenetv3. *Proceedings of the IEEE International Conference on Computer Vision*, 2019-October:1314–1324, 5 2019. ISSN 15505499. doi: 10.1109/ICCV.2019.00140. URL <https://arxiv.org/abs/1905.02244v5>.
- Andrew G. Howard, Menglong Zhu, Bo Chen, Dmitry Kalenichenko, Weijun Wang, Tobias Weyand, Marco Andreetto, and Hartwig Adam. Mobilenets: Efficient convolutional neural networks for mobile vision applications. 4 2017. URL <http://arxiv.org/abs/1704.04861>.
- Jie Hu, Li Shen, Samuel Albanie, Gang Sun, and Enhua Wu. Squeeze-and-excitation networks. *IEEE Transactions on Pattern Analysis and Machine Intelligence*, 42:2011–2023, 9 2017. ISSN 19393539. doi: 10.1109/TPAMI.2019.2913372. URL <https://arxiv.org/abs/1709.01507v4>.
- Matthew Inkawhich, Yiran Chen, and Hai Li. Snooping attacks on deep reinforcement learning. *Proceedings of the International Joint Conference on Autonomous Agents and Multiagent Systems, AAMAS*, 2020-May:557–565, 5 2019. ISSN 15582914. URL <https://arxiv.org/abs/1905.11832v2>.
- Marius F. R. Juston, William R. Norris, Dustin Nottage, and Ahmet Soylemezoglu. 1-Lipschitz Network Initialization for Certifiably Robust Classification Applications: A Decay Problem. 2 2025. URL <https://arxiv.org/pdf/2503.00240>.
- Diederik P. Kingma and Max Welling. An Introduction to Variational Autoencoders. *Foundations and Trends in Machine Learning*, 12(4):307–392, 6 2019. ISSN 19358245. doi: 10.1561/22000000056. URL <https://arxiv.org/pdf/1906.02691>.
- Günter Klambauer, Thomas Unterthiner, Andreas Mayr, and Sepp Hochreiter. Self-normalizing neural networks. *Advances in Neural Information Processing Systems*, 30, 2017.
- Laurent Lessard, Benjamin Recht, and Andrew Packard. Analysis and Design of Optimization Algorithms via Integral Quadratic Constraints. *SIAM Journal on Optimization*,

- 26(1):57–95, 10 2015. doi: 10.1137/15M1009597. URL <http://arxiv.org/abs/1408.3595><http://dx.doi.org/10.1137/15M1009597>.
- Andrew L. Maas, Y. Hannun Awni, and Andrew Y Ng. Rectifier nonlinearities improve neural network acoustic models. *Proceedings of the 30th International Conference on Machine Learning*, 28, 6 2013.
- Warren S. McCulloch and Walter Pitts. A logical calculus of the ideas immanent in nervous activity. *The Bulletin of Mathematical Biophysics*, 5:115–133, 12 1943. ISSN 00074985. doi: 10.1007/BF02478259/METRICS. URL <https://link.springer.com/article/10.1007/BF02478259>.
- Alexandre Megretski and Anders Rantzer. System analysis via integral quadratic constraints. *IEEE Transactions on Automatic Control*, 42(6):819–830, 1997. ISSN 00189286. doi: 10.1109/9.587335.
- Laurent Meunier, Blaise Delattre, Alexandre Araujo, and Alexandre Allauzen. A dynamical system perspective for lipschitz neural networks. *Proceedings of Machine Learning Research*, 162:15484–15500, 10 2021a. ISSN 26403498. URL <https://arxiv.org/abs/2110.12690v2>.
- Laurent Meunier, Blaise Delattre, Alexandre Araujo, and Alexandre Allauzen. A Dynamical System Perspective for Lipschitz Neural Networks. *Proceedings of Machine Learning Research*, 162:15484–15500, 10 2021b. ISSN 26403498. URL <https://arxiv.org/abs/2110.12690v2>.
- Laurent Meunier, Blaise J Delattre, Alexandre Araujo, and Alexandre Allauzen. A dynamical system perspective for lipschitz neural networks, 6 2022. ISSN 2640-3498. URL <https://proceedings.mlr.press/v162/meunier22a.html>.
- Diganta Misra. Mish: A self regularized non-monotonic activation function. *31st British Machine Vision Conference, BMVC 2020*, 8 2019. URL <http://arxiv.org/abs/1908.08681>.
- Takeru Miyato, Toshiki Kataoka, Masanori Koyama, and Yuichi Yoshida. Spectral normalization for generative adversarial networks. *6th International Conference on Learning Representations, ICLR 2018 - Conference Track Proceedings*, 2 2018. URL <https://arxiv.org/abs/1802.05957v1>.
- Victor Y. Pan and Zhao Q. Chen. Complexity of the matrix eigenproblem. *Conference Proceedings of the Annual ACM Symposium on Theory of Computing*, pages 507–516, 1999. ISSN 07349025. doi: 10.1145/301250.301389/ASSET/FC0FB8FD-669F-4EF9-B898-30A3DF5DA2BA/ASSETS/301250.301389.FP.PNG. URL <https://dl.acm.org/doi/pdf/10.1145/301250.301389>.
- Wei Ping, Kainan Peng, Andrew Gibiansky, Serkan O. Arik, Ajay Kannan, Sharan Narang, Jonathan Raiman, and John Miller. Deep voice 3: Scaling text-to-speech with convolutional sequence learning. *6th International Conference on Learning Representations*,

- ICLR 2018 - Conference Track Proceedings*, 10 2017. URL <http://arxiv.org/abs/1710.07654>.
- Bernd Prach and Christoph H. Lampert. Almost-orthogonal layers for efficient general-purpose lipschitz networks. 8 2022. URL <https://arxiv.org/abs/2208.03160v2>.
- Ed K R Rao and P C Yip. *The Transform and Data Compression Handbook*. CRC Press, 10 2018. ISBN 9781315220529. doi: 10.1201/9781315220529. URL <https://www.taylorfrancis.com/books/9781420037388>.
- Robin Rombach, Andreas Blattmann, Dominik Lorenz, Patrick Esser, and Bjorn Ommer. High-Resolution Image Synthesis with Latent Diffusion Models. *Proceedings of the IEEE Computer Society Conference on Computer Vision and Pattern Recognition*, 2022-June: 10674–10685, 12 2021. ISSN 10636919. doi: 10.1109/CVPR52688.2022.01042. URL <https://arxiv.org/pdf/2112.10752>.
- Olaf Ronneberger, Philipp Fischer, and Thomas Brox. U-Net: Convolutional Networks for Biomedical Image Segmentation. *Lecture Notes in Computer Science (including subseries Lecture Notes in Artificial Intelligence and Lecture Notes in Bioinformatics)*, 9351:234–241, 2015. ISSN 1611-3349. doi: 10.1007/978-3-319-24574-4{_}28. URL https://link.springer.com/chapter/10.1007/978-3-319-24574-4_28.
- Haşim Sak, Andrew Senior, and Françoise Beaufays. Long short-term memory based recurrent neural network architectures for large vocabulary speech recognition. 2 2014. URL <https://arxiv.org/abs/1402.1128v1>.
- Aliaksei Sandryhaila and Jose M. F. Moura. Eigendecomposition of block tridiagonal matrices. 6 2013. URL <https://arxiv.org/abs/1306.0217v1>.
- Sahil Singla, Surbhi Singla, and Soheil Feizi. Improved deterministic l2 robustness on CIFAR-10 and CIFAR-100. *ICLR 2022 - 10th International Conference on Learning Representations*, 8 2021. URL <https://arxiv.org/pdf/2108.04062>.
- Christian Szegedy, Sergey Ioffe, Vincent Vanhoucke, and Alexander A. Alemi. Inception-v4, inception-resnet and the impact of residual connections on learning. *31st AAAI Conference on Artificial Intelligence, AAAI 2017*, pages 4278–4284, 2 2016. ISSN 2159-5399. doi: 10.1609/aaai.v31i1.11231. URL <https://arxiv.org/abs/1602.07261v2>.
- Marco Taboga. Triangular matrix, 2021. URL <https://www.statlect.com/matrix-algebra/triangular-matrix>.
- Yusuke Tsuzuku, Issei Sato, and Masashi Sugiyama. Lipschitz-margin training: Scalable certification of perturbation invariance for deep neural networks. *CoRR*, abs/1802.04034, 2018. URL <http://arxiv.org/abs/1802.04034>.
- Ruigang Wang and Ian R. Manchester. Direct Parameterization of Lipschitz-Bounded Deep Networks. *Proceedings of Machine Learning Research*, 202:36093–36110, 1 2023. ISSN 26403498. URL <https://arxiv.org/pdf/2301.11526>.

- David S. Watkins. *Gaussian Elimination and Its Variants*, pages 1–110. Wiley, 5 2002. ISBN 9780471249719. doi: 10.1002/0471249718.ch1. URL <https://onlinelibrary.wiley.com/doi/10.1002/0471249718.ch1>. Wiley Online Books.
- Ezra Winston and J. Zico Kolter. Monotone operator equilibrium networks. *Advances in Neural Information Processing Systems*, 2020-December, 6 2020. ISSN 10495258. URL <https://arxiv.org/pdf/2006.08591>.
- Max A Woodbury. *Inverting modified matrices*. Princeton University, Princeton, NJ, 1950.
- Saining Xie, Ross Girshick, Piotr Dollár, Zhuowen Tu, and Kaiming He. Aggregated residual transformations for deep neural networks. *Proceedings - 30th IEEE Conference on Computer Vision and Pattern Recognition, CVPR 2017*, 2017-January:5987–5995, 11 2016. doi: 10.1109/CVPR.2017.634. URL <https://arxiv.org/abs/1611.05431v2>.
- Bing Xu, Naiyan Wang, Tianqi Chen, and Mu Li. Empirical evaluation of rectified activations in convolutional network. 5 2015. URL <http://arxiv.org/abs/1505.00853>.
- Yuezhu Xu and S. Sivaranjani. Eclipse: Efficient compositional lipschitz constant estimation for deep neural networks. 4 2024. URL <https://arxiv.org/abs/2404.04375v2>.
- Sergey Zagoruyko and Nikos Komodakis. Wide residual networks. *British Machine Vision Conference 2016, BMVC 2016*, 2016-September:87.1–87.12, 5 2016. doi: 10.5244/C.30.87. URL <https://arxiv.org/abs/1605.07146v4>.
- Mingyuan Zhou. Softplus regressions and convex polytopes. 8 2016. URL <http://arxiv.org/abs/1608.06383>.